Production of Bio-based Lactone Monomers for Intrinsically Recyclable Plastics

By

Lucas A. Baston

B.S.E Chemical Engineering, Purdue University, 2020

Submitted to the Department of Chemical Engineering in partial fulfillment of the requirements for the degree of

Master of Science in Chemical Engineering

At the

Massachusetts Institute of Technology

May 2024

Authored by: Lucas A. Baston

Department of Chemical Engineering

May 16, 2024

Certified by: Yuriy Román-Leshkov

Robert T. Haslam (1911) Chair of Chemical Engineering

Professor of Chemical Engineering

Thesis Supervisor

Accepted by: Hadley D. Sikes

Willard Henry Dow Professor of Chemical Engineering

Graduate Officer

Production of Bio-based Lactone Monomers for Intrinsically Recyclable Plastics

By

Lucas A. Baston

Submitted to the Department of Chemical Engineering in partial fulfillment of the requirements for the degree of

Master of Science in Chemical Engineering

At the

Massachusetts Institute of Technology

May 2024

Abstract

The development of intrinsically recyclable plastics is crucial to halt the accumulation of waste plastics in the environment. While great strides have been made in the design of novel polymers that exhibit desirable qualities and degrade back to their respective monomer at mild conditions, the development of scalable synthesis of the monomers for these plastics lags behind. This work aims to develop methods for the synthesis of monomers using heterogeneous catalysts to allow for scaling-up. First, we used a high-throughput computational method to screen binding energies of key reaction species of more than 200 zeolite frameworks to identify potential catalysts that would selectively catalyze our probe reaction of methyl lactate lactonization to lactide. From these computations, we identified titanium-containing zeolite with the MEL topology as a promising catalyst for this reaction in the gas phase. Continuous-flow kinetic studies revealed that Ti-MEL showed 40% increased selectivity to the lactide product at over twice the conversion as Ti-BEA and Ti-MFI. Second, we show a potential pathway for the production of α-cyclohexyl-δ-valerolactone (CVL) starting from formaldehyde and δ-valerolactone (DVL). We developed a continuous gas-phase reactor using alkaline earth oxides supported on silica as catalysts for an aldol condensation reaction. CaO and BaO showed 90% and 83% selectivity, respectively, to α-methylene-δ-valerolactone at 60% DVL conversion. Following this, MVL was functionalized with 1,3-butadiene in a Diels-Alder addition to form the unsaturated form of our desired CVL monomer (CeVL). This reaction was catalyzed over Lewis acid with selectivities reaching 90% of Sn-BEA catalysts at mild temperatures of 55 °C. Finally, the CeVL was able to be hydrogenated to CVL over commercially available palladium on carbon catalysts with flowing hydrogen.

Thesis Supervisor: Yuriy Román-Leshkov

Title: Robert T. Haslam (1911) Chair of Chemical Engineering, Professor of Chemical Engineering

Table of Contents

Abstract 3
Table of Contents 4
List of Figures, Schemes, and Tables 6
1. Background and Motivation 8
1.1 Introduction to Zeolites as Catalysts 8
1.2 Rational Selection of Zeolites 10
1.3 Transition State Mimics 10
1.4 Next-Generation Plastics 11
2. Gas Phase Lactonization of Methyl Lactate 12
2.1 Executive Summary 12
2.2 Approach 12
2.3 Methods 14
2.3.1 Synthesis Procedures 14
2.3.2 Catalyst characterization 14
2.3.3 Chemical Quantification 15
2.3.4 Reactor Configuration and Operating Procedure 15
2.4 Results 16
2.4.1 Docking Simulations 16
2.4.2 Catalyst Characterization 16
2.4.3 Kinetic Studies 17
2.5 Future Work – Gas Phase Lactonization Study 20
3. Developing new pathways to critical CVL monomers 22
3.1 Executive Summary 22
3.2 Approach 22
3.3 Methods 23
3.3.1 Catalyst Synthesis 23
3.3.2 Catalyst Characterization 24
3.3.3 Chemical Quantification 24
3.3.4 Reactor Configuration(s) and Procedure 24
3.4 Catalyst Screening for the Gas-Phase Production of MVL 25
3.4.1 Catalyst Characterization 25
3.4.2 Catalyst Screening for the Gas-Phase Production of MVL 26
3.4.3 Catalyst Screening for Conversion of MVL to CeVL 27

3.4.4 Conversion of CeVL to CVL 29
3.5 Future work for DVL to CVL pathway optimization 30
4. Conclusion 30
5. Acknowledgements 31
Appendix: Supplementary Figures 33
References 45

List of Figures, Schemes, and Tables

Figure 1: Increasing Complexity of Zeolite Building Units 8

Figure 2: Templating Effects of OSDAs..... **Error! Bookmark not defined.**

Figure 3: Binding Energies of Lactide for Selected Zeolite Frameworks..... 13

Figure 4: Comparison of different zeolite frameworks (~100 mg) for the production of lactide at 250 °C and a WSHV of 15 $g_{ML}\ g_{cat}^{-1}\ h^{-1}$. Feed was 15 wt% methyl lactate, 1 wt% o-xylene, and balance dioxane at 0.15 mL min^{-1} to reach a WSHV of 15 $g_{ML}\ g_{cat}^{-1}\ h^{-1}$. Each vertical bar represents a different sample taken approximately 20 min apart. Ti-MEL-OH was first run at a WHSV of 15 $g_{ML}\ g_{cat}^{-1}\ h^{-1}$ before increasing to 20 $g_{ML}\ g_{cat}^{-1}\ h^{-1}$ for the fifth data point and beyond..... 19

Figure 5: Data from additional docking simulations. a) Shows Lactide binding energies. b) Shows Dimer Binding Energies c) Shows trimer binding energies (docking not possible for FER). d) Shows the change in binding energy for the lactonization step (Dimer to Lactide in Scheme 1). e) Shows the change in binding energy for the overall reaction (e.g., binding energy of lactide – twice the binding energy of methyl lactate). f) Shows the change in binding energy for the trimerization step (Dimer to Trimer in Scheme 1)..... 21

Figure 7: Product distributions and DVL conversions as functions of contact time for (a) MgO/SiO_2, (b) CaO/SiO_2 and (c) BaO/SiO_2 (613 K, 0.1 g catalyst, 0.4 kPa DVL, 1.2 kPa FA, 101 kPa total pressure with balance N_2)..... 27

Scheme 1: Reaction pathway towards the lactonization of methyl lactate 13

Scheme 2: Aldol Condensation of DVL and Formaldehyde 22

Scheme 3: Diel-Alder addition of 1,3 butadiene to MVL followed by hydrogenation to form CVL..... 23

Table 1: Initial conversions and selectivities for the lactonization of methyl lactate to lactide as a function of temperature. All reactions were run with neat methyl lactate feed (0.15 mL min^{-1}) and ortho-xylene internal standard under N_2 flow (60 mL min^{-1}) and ~600 mg of catalyst with WHSV ~11 $g_{ML}\ g_{cat}^{-1}\ h^{-1}$.... 17

Table 2: Feed recycle study over Ti-MFI-OH, Ti-MEL-OH, and De-Al-BEA. First pass feed was comprised of 15 wt. % methyl lactate, 1 wt% o-xylene, and balance dioxane. WHSV for titanium-containing zeolites during both passes were 15 $g_{ML}\ g_{cat}^{-1}\ h^{-1}$ (feed flow rate of 0.15 mL min^{-1} and ~100 mg catalyst). 20

Table 3: Weight loadings of metal oxides on silica 26

Table 4: Si:M ratios and TOF for the production of CeVL over various catalysts. All reactions run in sealed glass reactor vials under constant stirring at ambient temperature. Reactor vials contained 200 µL MVL, 50 µL p-xylene, and 2 mL of 20 wt. % 1,3-butadiene in toluene. Approximately 50 mg of sample were added

for all heterogeneous catalysts. An equivalent about of Sn to the Sn-BEA-F experiment was added for the $SnCl_2$ experiment, rather than 50 mg. Reactions were run overnight. 28

Table 5: Temperature study of CeVL reaction. Each reaction vial was loaded with 100 mg of catalyst, if present, 200 μL of MVL, 100 μL of p-xylene, 2 mL of 20 wt. % 1,3-butadiene in toluene, and a magnetic stir bar. The reaction was allowed to proceed for 86 h with samples taken at 11, 18, and 45 h with the method described in section 3.3.4. Final MVL conversions and CeVL selectivity were calculated from the final time point. 29

1. Background and Motivation

1.1 Introduction to Zeolites as Catalysts

The term 'zeolite' was first coined over 260 years ago in 1756 by Swedish mineralogist Axel Fredrik Cronstresdt to describe a natural mineral he discovered that, when heated, released steam.[1] Zeolites are aluminosilicate materials comprising of tetrahedrally coordinated silicon and aluminum atoms linked by oxygen bridges (i.e. SiO_4 and AlO_4).[2] From these tetrahedral units, secondary building units (SBUs) such as rings and cages are formed, which coalesce to form the defining crystal structure of the zeolite framework as shown in Figure 1. Frameworks are each given a three-letter identifying code such as MFI, BEA, or MOR. The SBUs form channels and cavities that can range in size from 3-15 Å allowing the uptake of guest molecules.[3] This complex internal structure of zeolites has given them separation capabilities relevant to ion exchange in water purification[4] and selective sorption for carbon capture technologies.[5] The introduction of non-silicon atoms into the framework gives these frameworks acidic properties that allow them to function as heterogeneous catalysts.

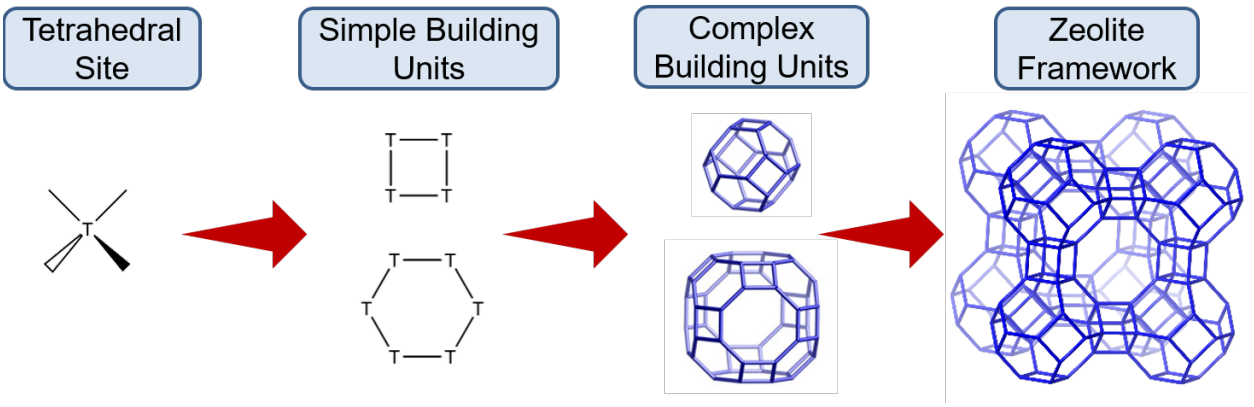

Figure 1: Increasing Complexity of Zeolite Building Units

Since their discovery, zeolites have become an indispensable material, with a market valuation of $12.1 billion in 2021.[6] In particular, zeolites have become a staple of processes in the petrochemical, fine chemical synthesis, and automotive pollution abatement industries.[7-9] Key to this success is their microporous environment that can vary between frameworks and allow for exclusion based on the size of reactants, product, or transition states.[2] Currently, there are over 250 experimentally verified zeolite frameworks,[10] and theorical predictions estimate more than 2 million viable framework structures are possible.[11] Despite this, only 13 frameworks are used commercially due to their inexpensive synthesis procedures and the fact that they cover a sufficient range of pore sizes for most size exclusion applications.[12]

While pure-silica zeolites containing no heteroatoms have been prepared, applications require isomorphic substitution of other elements as. The lack of charge imbalance or electron density variation limits the use of pure-silica materials as catalysts, though they are still useful as adsorbents and sieves. The most common change to pure-silica frameworks is the incorporation of aluminum which results in a net negative charge that must be balanced by an extra-framework cation, which can include protons, generating Brønsted acid sites. Beyond aluminosilicates, many additional 'zeotypes' exists that use a wide variety of elements to provide unique properties. Other aliovalent elements can be included, such as boron, to create weaker Brønsted acid sites than aluminum,[13] or gallium, which can form large, 18 membered rings in the framework

unobserved in other zeotypes.[14] Another class of zeotypes are those where the heteroatom is isovalent with silicon, such as titanium, tin, or hafnium. In these cases, there is no charge imbalance that must be counteracted with extra-framework cations, but the partial positive charge of these metals that arises upon binding with neighboring oxygen atoms allows for the acceptance of electron density, also known as Lewis acidity.[15]

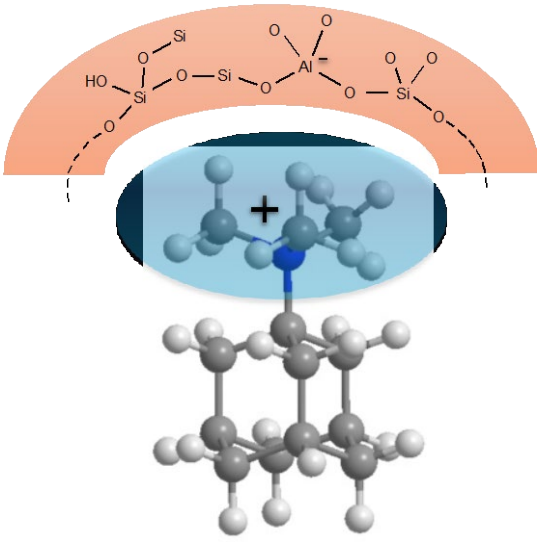

Figure 2: Templating Effects of OSDAs

Hydrothermal synthesis of zeolites, first developed by Barrer, et. al.,[16-17] is the most studied and widely used method,[3] though other approaches such as dry-gel conversion[18] and microwave synthesis[19] have been reported. In a standard hydrothermal synthesis, an aqueous medium containing a mineralizing agent, structure-directing cations, and sources for tetrahedral atoms are placed inside of a polytetrafluoroethylene (PTFE) vessel inside a stainless-steel autoclave, sealed to allow for natural pressurization, and heated to 100-200 °C. The time period for this synthesis can range on the order of hours to months depending on the specific synthesis conditions and target framework. Synthesis in alkali-hydroxide media allows for effective precursor dissolution, but the high-degree of cations necessitated to reach high pH leads to aluminum-rich frameworks.[20] Alternately, use of an organic structure directing agent (OSDA) allows for higher silicon content via reduced cations, with the added benefit of the OSDA "templating" the resultant framework.[21] The exact nature of zeolite synthesis and how this templating occurs is not well understood due to the large number of variables present and the complexity of the process. Burkett and Davis propose a model for synthesis in which organic-inorganic complexes form though non-covalent bonding and mimic the interactions and shape of the occluding OSDA in the final zeolite framework.[22] Gies and Marker[23] note correlations between size and shape of the OSDA and the resulting zeolite void space, indicating a strong templating effect from van der Waals forces as shown in Figure 2.

Zeolites may exhibit other synthesis-derived properties independent of framework templating through altering the electrostatic interactions between structure directing agents and the framework. For example, through the use of different (or combinations of) structure directing agents, the location and distribution of aluminum sites in the framework can be altered. This active site distribution can in turn affect how the rate of reactions such as methanol dehydration[24] and methanol to olefin (MTO) reactions.[25] Alternatively, the positive charge of the structure directing agent can be balanced either by aluminum incorporation into the framework at a tetrahedral site (T-site) as seen in Figure 2 or through the formation of broken Si-O-Si bonds that can later form silanol (-Si-O-H) nests.[26] At a fixed Si/Al ratio, the number of silanol defects in the framework can be reduced by the use of fluoride anions as the mineralizer. In these systems, typically at neutral to slightly alkaline pH, the fluoride anion can direct the formation of small cages and balance out cations from the SDAs from within these cages.[27] The presence of defects within the framework can have a substantial role on the catalytic activity of the final zeolite through the organization of solvent molecules within the pores through the effects of molecular clustering and extended solvent networks.[28-30]

1.2 Rational Selection of Zeolites

The confining structure of zeolites has been studied for its ability to influence reactions in a manner similar to a "solid solvent."[31] The tighter the molecular confinement, the stronger the attractive van der Waals forces become (up to the point of exclusion),[32] leading to more negative adsorption enthalpies and entropies. These effects have led to comparisons between the confining voids of zeolites and biological enzymes due to their shared ability to stabilize transition states beyond the active site, drastically enhancing reaction rates.[33-34] Harris et. al.[35] showed that the rates for aqueous glucose isomerization over Lewis acid sites could increase up to four orders of magnitude changing from unconfined Sn-xerogel to Sn-BEA zeolites. Similarly, rate constants for cyclohexene epoxidation improved 5-fold (on a Ti atom basis) within the cavities on the external surface of *-SVY zeotypes when compared to Ti on an amorphous silicon support.[36] Confinement effects arise from shifting the balance of enthalpic bonuses and entropic penalties and are therefore framework-dependent.[37] Bregante et. al. demonstrated styrene epoxidation rates over titanium zeolites are fastest in Ti-FAU due to more favorable enthalpic interactions (than amorphous silica) but a lower entropic penalty (than tighter-binding BEA).[38] Cordon et. al.[39] studied how glucose isomerization can be preferentially directed to fructose or sorbose based on the selected framework, despite both reactions occurring simultaneously.

Framework selection is generally dictated by availability, as zeolite synthesis is difficult and production of new zeolite frameworks relies on a mixture of trial-and-error and chemical intuition to guide modification of synthesis conditions and selection of new OSDAs. The specific zeolite chosen to catalyze a reaction is extremely important, but most of the studies listed above focus on the commercially relevant frameworks, which are unlikely to be optimal for any given reaction.

1.3 Transition State Mimics

One method that has been used to great success to optimize the interaction between transition states and the confining voids while avoiding adherence to only the commercially relevant frameworks is the use of transition-state mimics. In this process, a zeolite is templated using an OSDA that closely matches the shape of the transition state of the reaction in question. Since the OSDA is essential in templating the voids of the zeolite during synthesis, the resulting shape of the pore or cavity in the zeolite post calcination of the OSDA should stabilize the transition state the of the reaction the OSDA is attempting to mimic. Through this process, Li et. al.[40] were able to synthesize a zeolite with the RTH framework that produces a 3-fold higher propylene to ethylene ratio in MTO reactions than a standard CHA framework. A similar study by Gallego et. al.[41] used a zeolite catalyst with the IWV framework for ethylbenzene isomerization to xylenes that was prepared with an OSDA that closely mimicked the transition state of the reaction. While the IWV zeolite had an overall lower conversion when compared to the commercial MOR framework (26% versus over 70%), the selectivity towards xylene products was over 3-fold higher for the mimic zeolite at the same conditions and more than twice as high when compared at the same conversion.[41]

While transition state mimic zeolite synthesis has shown to be effective, it relies on human knowledge to find organic molecules closely resembling the transition state of interest. In an effort to increase the applicability of this methodology, a computational method for running the high-throughput calculations of host-guest interactions in zeolite pores was developed through collaborations with the MIT materials science department, specifically the Gómez-Bombarelli and Olivetti Groups. This method was initially developed to identify alternative OSDAs for zeolite synthesis to reduce costs and potentially expand synthesis windows. This is done through Drieiding force field calculations to determine the binding energies between a zeolite framework and a guest molecule.[42] Zeolites and guest molecules are first optimized separately, then docked and frozen for energy estimation, producing a binding energy with accuracy comparable to density functional theory-molecular dynamics (DFT-MD) simulations.[42] While the

agreement is not exact with DFT-MD, it is orders of magnitude faster to compute these calculations, allowing the technique to be applied to a wide range of molecules and zeolite frameworks in a rapid screen. The tool provides a templating energy derived from the relative affinity of the OSDA to this framework when compared across other frameworks it may template as well as the relative binding potential of this molecule compared to all other potential templating molecules simulated by this tool.

Schwalbe-Koda and Kwon et. al. employed this computational method to find an alternative synthesis of CHA which replaces the expensive OSDA trimethyl adamantylammonium with the more attainable 6-azaspiro[6,5]dodecan-6-ium.[43] The success of this tool in finding a replacement OSDA led us to extend its use to the identification of potential zeolite frameworks that would improve the selectivity and activity of a reaction of choice, following a similar strategy to the transition state mimic studies discussed previously, but with a much wider scope of molecules and frameworks.

1.4 Next-Generation Plastics

One of the greatest problems facing mankind at the moment is the accumulation of plastic waste in the environment. By 2050, the production of synthetic polymers is expected to reach 1.12 billion tons per year.[44] The majority of plastics produced today are derived from non-renewable fossil fuels in a linear economy – fossil fuels are extracted, made into polymers, used , and disposed of through landfilling, incineration, or marine dumping.[45] Common plastics, designed for durability, can take $10^6 – 10^7$ years to fully decompose, leading to continuous environmental accumulation.[46] Current global recycling efforts sit at around 18% for non-fiber plastics[47], though common mechanical recycling techniques have a cycle limit and may lower the value and quality of recycled materials.[48]

Recent efforts have been made to develop intrinsically recyclable or intrinsically circular polymers (iCPs), which are designed specifically to easily depolymerize back into monomers under relatively mild conditions in the presence of a catalyst. Returning to pure monomer could avoid the loss in quality caused by mechanical recycling. To accomplish this recyclability, the iCP must have a low ceiling temperature (T_c), defined as the temperature at which the entropy loss from polymerization balances out the enthalpic gain.[49] Thus, a polymer at its ceiling temperature would be in equilibrium between polymerization and depolymerization, and higher temperatures would result in thermodynamically favorable depolymerization to monomers. Naturally, polymers with low T_c could be unstable at working or processing conditions without a significant kinetic limit preventing depolymerization. To avoid this, these iCPs are "kinetically trapped" through intrinsic properties of the polymer or functionalized end caps that must be removed before depolymerization will proceed, enabling high working temperatures for these low T_c polymers.[50]

In the pursuit of new iCPs, focus has been on the design of the monomers.[50] Lactones, cyclic esters, are promising candidates due in part to the ring strain acting as a driving force for ring-opening polymerization (ROP). Early examples of ROP applied to bioderived plastics were polyglyocolic acid (PGA), polylactic acid (PLA), and their copolymer (PLGA) due to their biocompatibility and biodegradability.[51] Initial attempts at polymerization of these monomers through polycondensation resulted in low molecular weight and poor polydispersity due to the equilibrium of the reaction, the difficulty of water removal, and poor stereoregularity.[52] Using ROP circumvents these issues, enabling commercial PLA production with useful properties.[53]

However, PLA is not the ideal polymer for depolymerization due to undesired transesterification occurring during depolymerization, creating racemic mixtures and cyclic oligomers which prevent re-polymerization to isotactic PLA.[54] Work by Hong and Chen[55] has shown the ROP of γ-butyrolactone and subsequent depolymerization at ambient conditions to pure monomer, which could allow for the production of other polymers based on this five-membered ring backbone. Another promising candidate for ROP is the cyclic

dimer of 3-hydroxybutyric acid (3HB) to poly(3-hydroxybutyrate) (P3HB). This polymer can be naturally derived and a recent catalyst design by Tang and Chen[56] has shown the ability to form fully isotactic P3HB from a racemic mixture of the cyclic diolide.

In order to explore the potential of these intrinsically recyclable polymers derived from ROP, novel lactone monomers must be produced. Often the production of such monomers is challenging. In the case of P3HB, current synthesis of the dilactone involves multiple intermediates, strongly acidic conditions, and multiple solvent evaporation steps.[56] Industrial synthesis of lactide for the ROP to PLA involves a two-step process of oligomer formation and backbiting.[52] In the case of lactide synthesis, one-step processes within zeolite pores have been investigated and show to work.[52] This created an opportunity for us to apply the computational tool to rationally select zeolite frameworks that showed promise in catalyzing reactions towards monomers of intrinsically recyclable plastics.

2. Gas Phase Lactonization of Methyl Lactate

2.1 Executive Summary

In this study, we chose the synthesis of lactide from methyl lactate as a probe reaction to test our hypothesis that we can rationally select a zeolite framework to increase the selectivity of a reaction using high-throughput docking simulations. We docked the lactide product molecule in all zeolite frameworks, though some frameworks did not have large enough pores to accommodate the molecule, leading to a failed simulation. From the successful simulations, we identified MEL as a potential candidate to increase the selectivity of this reaction compared to previously studied MFI and BEA due to its more favorable binding to lactide. After synthesizing MEL, MFI, and BEA catalysts, gas-phase reaction studies were performed over a range of temperatures and WHSV. We demonstrated that titanium-containing MEL showed improved selectivity towards lactide at similar conversions compared to titanium-containing BEA and MFI.

2.2 Approach

To focus on a chemistry relevant to next-generation monomers for ROP, the production of lactide was selected as a probe reaction with Ti-based Lewis acidic zeolites. Specifically, the methyl ester form of lactic acid (methyl lactate) was used, as its lower boiling point allows for gas-phase reactions, enabling facile study of kinetics in flow as well as parity with the (solvent-free) docking simulations. The reaction is shown in Scheme 1. Conveniently, the reactants and products are commercially available for improved quantification. Regarding the Ti-based catalysts, Previous studies on the production of lactide (LD) have shown high selectivity over titanium oxide supported on silica acting as Lewis acid catalysts.[57] Through both direct synthesis and post-synthetic grafting, it is possible to incorporate titanium directly into the silica zeolite framework to not only mimic these catalysts but also introduce confinement effects from the zeolite framework. As shown in De Clercq et. al.,[57] using titanium-containing zeolites as the catalyst rather than titanium oxide on amorphous silica led to higher per-site rates in the dimerization and lactonization of methyl lactate (ML), proposing the tetrahedral titanium sites in these zeolites to be more active than the titanium oxide oligomers found in the supported catalysts.

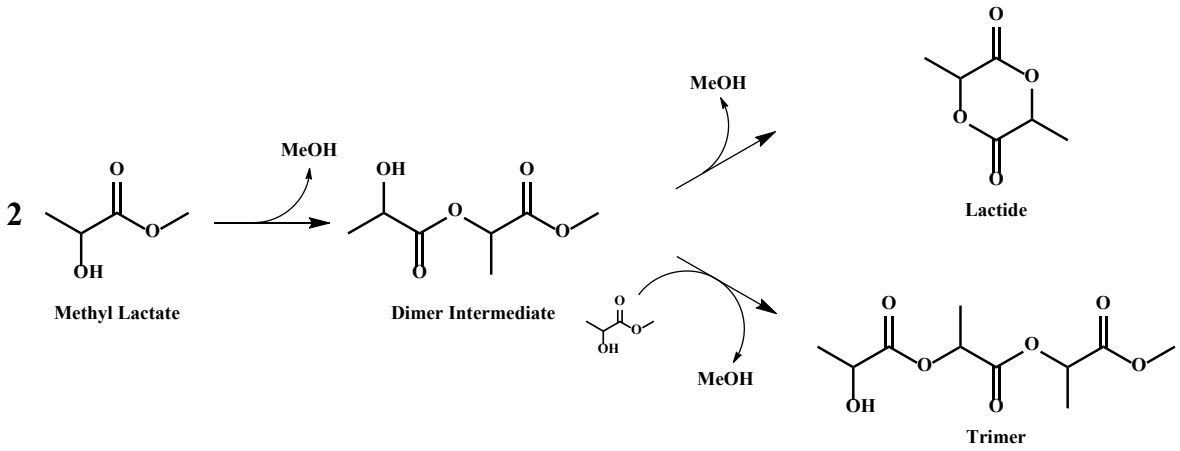

Scheme 1: Reaction pathway towards the lactonization of methyl lactate

Docking simulations with lactide as the guest molecule, used as a proxy for the transition state following Hammond's postulate for this endothermic reaction, were performed for over 200 frameworks (*vide infra*). In addition to the commercial frameworks of BEA and MFI, included as a benchmark, simulations identified MEL as a promising framework as it is well-studied while also showing relatively more favorable binding energies towards lactide. We hypothesized this more favorable binding energy would lead to higher selectivity of lactide employing a MEL zeolite catalyst versus BEA or MFI.

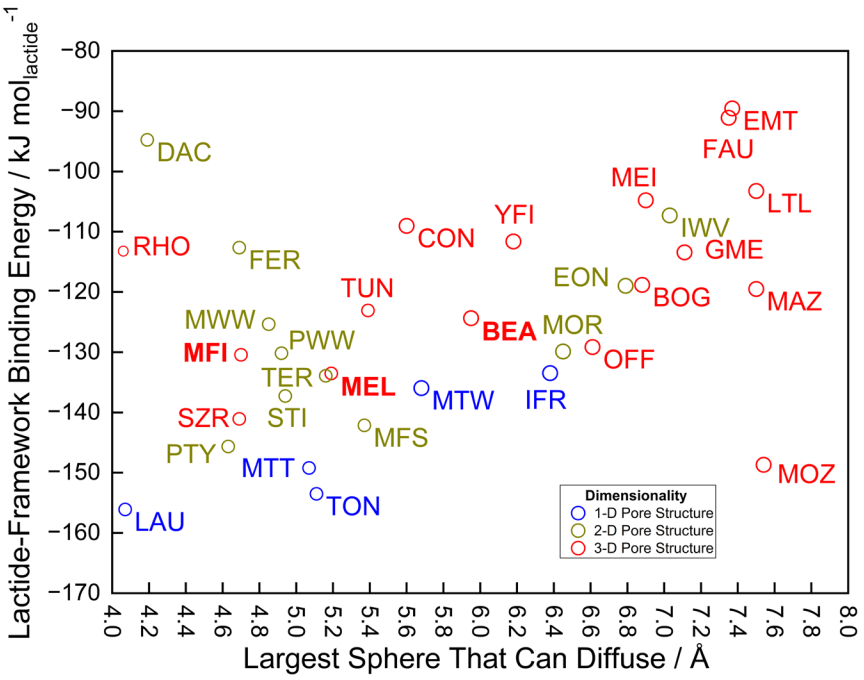

Figure 3: Binding Energies of Lactide for Selected Zeolite Frameworks

2.3 Methods

2.3.1 Synthesis Procedures

Hydrophobic titanium beta (Ti-BEA-F) was synthesized by prior members of the lab following procedures outlined in Camblor et. al.[58] with titanium (IV) chloride (99%, Sigma Aldrich) rather than the listed tin (IV) chloride hydrate. New Ti-BEA-F materials were not synthesized for this project.

Hydrophilic titanium MFI (Ti-MFI-OH) was synthesized following the method outlined in De Clerq et. al.[57] In an example synthesis, 2.43 g tetrapropylammonium hydroxide (TPAOH; 40 wt.% in water, Merck Chemical), 6.00 g tetraethyl orthosilicate (TEOS; 99%, Sigma Aldrich), 0.11 g titanium (IV) ethoxide (TEOT; technical grade, Sigma Aldrich), and 6.80 g of Milli-Q water (18.2 MΩ, from Barnstead Nanopure unit) were added to a PTFE mixing vessel with a PTFE-lined magnetic stir bar. This mixture was heated to 40 °C uncovered for 3 hours to allow for the TEOS to hydrolyze. After this, 11.99 g of additional Milli-Q water was added and the mixture was homogenized. This mixture was transferred to a PTFE liner placed inside a stainless-steel autoclave. The final molar gel ratio was targeted at 1.00 SiO_2 : 0.017 TiO_2 : 0.2317 TPAOH : 39.41 H_2O. This gel was heated, under constant rotation, in a 180 °C for 15 hours.

Hydrophilic titanium MEL (Ti-MEL-OH) was synthesized following the method outlined in Reddy et. al.[59] In an example synthesis, 5.92 g tetrabutylammonium hydroxide (TBAOH; 25 wt. % in methanol, Sigma Aldrich) and 8 g TEOS were added to a PTFE vessel with a PTFE-lined magnetic stir bar and mixed for 30 minutes at room temperature. Following this, a solution composed of 0.133 titanium (IV) butoxide (TBO; 97%, Sigma Aldrich) and 1.15 g isopropyl alcohol (IPA; 99%, Sigma Aldrich) was added to the mixing vessel dropwise while continuously stirring. An additional 1.97 g of TBAOH was added while mixing and the resulting gel was allowed to stir, uncovered, for 4 hours at 60 °C. 16.00 g of Milli-Q water was added and mixed for 30 minutes. The resulting zeolite gel, with a molar composition of 1.00 SiO_2 : 0.01 TiO_2 : 0.20 TPAOH : 20.00 H_2O, was transferred to a PTFE-lined stainless-steel autoclave. This autoclave was placed in a convection oven at 170 °C for 2 days under continuous rotation.

Following synthesis, the zeolites were removed from the liners and transferred to centrifuge tubes. These were run at 1100 rpm for at least 5 minutes, or until the supernatant liquid was clear. The supernatant liquid was removed and the zeolites were washed with clean Milli-Q water and separated via centrifugation again. This process was repeated until the pH of the supernatant liquid was neutral. Following washing, the zeolites were dried at 100 °C in air and then calcined under flowing air at 580 °C for 5 hours.

Dealumination of commercial BEA catalysts (Zeolyst, CP814E) was performed in a 500 mL glass round-bottom flask with attached condenser. Approximately 2 grams of BEA was added to 250 mL of 70 wt. % nitric acid (Fisher Scientific). This was stirred with a PTFE-lined magnetic stir bar at 500 rpm and 80 °C overnight. Following this, the mixture was allowed to cool to room temperature and the zeolite was separated via centrifugation. The supernatant fluid was disposed of and replaced with fresh Milli-Q water before washing and separating. This process was repeated until the supernatant fluid reached a constant pH. The zeolites were dried overnight at 100 °C followed by calcination in flowing air at 580 °C for 5 hours. Prior to calcination, the de-aluminated samples appeared reddish-brown but were white post-calcination.

2.3.2 Catalyst characterization

The crystallinity of the zeolite catalysts was confirmed using powder x-ray diffraction collected using a Bruker D8 diffractometer using Cu-Kα radiation (λ=1.5418 Å, 40 kV, 40 mA) and a slit size of 2 mm. Intensity data was recorded on a 2θ range of 5-50° with angular step size of 0.02° and a scanning rate no faster than 5° min^{-1}. Patterns were compared to reference patterns obtained from the IZA database.[10]

Silicon, alumina, and titanium contents of the catalysts were determined using inductively coupled plasma atomic emission spectroscopy (ICP-AES, Agilent 5100). Approximately 5 mg of solid catalyst was added to a centrifuge tube along with 1 mL Milli-Q water, 0.2 mL hydrofluoric acid (48 wt. %, trace metals basis, Sigma Aldrich), and 0.3 mL nitric acid (68%, Veritas double-distilled, GFS Chemicals) and mixed vigorously. The catalyst was allowed to digest for at least 1 hour before 6 mL of 4 wt. % boric acid in water (99.5%, reagent grade, Sigma Aldrich) was added to neutralize the hydrofluoric acid. The solution was diluted to 10 mL with Milli-Q water. Metal concentrations were determined from calibration curves prepared from standard solutions of 1000 ppm of Si, Al, and Ti (all TraceCERT, Sigma-Aldrich), diluted in 2 wt. % HNO_3.

Scanning electron microscopy (SEM) was performed on a Zeiss-Merlin High-resolution SEM. Samples were prepared into a fine powder and loaded on carbon black tape. Images were collected at 2.0 kV, 100 pA, and 6.6 mm WD with HE-SE2 detector.

Diffuse reflectance UV–Vis spectra were measured on a Cary 5000 spectrometer (Agilent) equipped with a DiffusIR diffuse reflectance accessory and environmental chamber (PIKE Technologies). UV–Vis spectra were collected on zeolite samples at 25 °C after dehydration at 250 °C under flowing dry air for 2 h and measured relative to a barium sulfate ($BaSO_4$; 99 wt. %, MilliporeSigma) background.

2.3.3 Chemical Quantification

Reaction products were quantified using an Agilent 7890 Gas Chromatography Unit with a HP-5 column. Standard solutions of ortho-xylene ortho-xylene (98%, Sigma Aldrich), methyl-S-lactate (97%, Acros Organics) and L,L-lactide (98%, TCI) in acetone (99.5%, Sigma Aldrich) were prepared to create standards relative to ortho-xylene. Response factors for the linear dimer and trimer of methyl lactate were estimated following the procedure outlined in Scanlon et. al.[60] Unknown products were identified using an Agilent 7820A CS with 5977B Mass Selective Detector (MSD) equipped with an Agilent HP5 MS-UI 30 m column (0.25 mm diameter, 0.25 μm film thickness).

2.3.4 Reactor Configuration and Operating Procedure

The plug-flow, gas-phase reactor for this study (Outlined in Figure A-1) was constructed from Swagelok fittings and 316 stainless-steel tubing sourced from McMaster-Carr. Liquid was fed from a vessel placed on a scale and zeroed before the reaction started to measure the mass flow rate into the system. Liquid was pumped through an Acuflow Series II high-pressure liquid chromatography (HPLC) pump. Nitrogen carrier gas was fed into the reactor using Brooks 4840 E mass flow controllers with a pressure gauge upstream of the reactor. A gas-phase feed was produced by mixing the liquid feed with the gas feed prior to the reactor bed using a bored-through union to surround the liquid with N_2 in a heated portion of the furnace. The reactor (1/4” O.D., 316 stainless steel tube) was kept isothermal inside a furnace (Applied Test Systems) fitted with custom steel heating blocks in contact with both the reactor tube and a K-type thermocouple (fitted into a groove in the block) attached to a temperature controller (Cole-Parmer Digi-Sense R/S 68900-11). Inside the reactor, the catalyst bed consisted of mixed sieved zeolite (250-500 μm) and inert silicon carbide (120 grit, Alfa Aesar) trapped between pieces of quartz wool. Borosilicate glass beads (1 mm) were packed above and below the bed for support, assisting with vapor heating, and to limit dead volume. Downstream of the reactor, heated lines (>210 °C, controlled with BriskHeat 6’ x 1/2” heating tape controlled via Glas-Col PowrTrol variable voltage regulator with temperatures measured by external K-type thermocouples) transported vapor to a gas-liquid separator (Jerguson). Valves before and after the separator allowed for liquid sampling during reaction without major disruption of gas flow. Gas flow post-separator was variously vented or directed to a bubble flow meter for direct flow measurement. Pressure gauges before and after the reactor were used to assess pressure drop, which was kept below 10 psi for all experiments.

All reactions in this study were run under atmospheric conditions with carrier gas flow rates between 10-100 mL min^{-1} as measured by a bubble flow meter. Inlet liquid feed flow (HPLC pump volumetric set point 0.1-0.5 mL min^{-1}) was determined using a scale and timer to determine the average mass flow into the system during a sample collection period, typically 20-30 minutes. Reaction temperatures were controlled between 220 and 280 °C. Catalyst bed loadings ranged from 100 to 600 mg, with a SiC dilution ratio of 1 to 5 when working with 100 to 200 mg of catalyst, computing WHSV based on the inlet feed mass flow and the mass of catalyst measured during bed preparation ($g_{Methyl\ Lactate}\ g_{cat}^{-1}\ h^{-1}$). Controls indicated SiC was not catalytically active. Prior to reactions, the catalyst bed was pre-treated in flowing air (>100 mL/min) at 500 °C for 6 h. Mass recovery was calculated by comparing the mass flow into the system and the mass collected at each sampling point. Typically, the first 60 minutes of a reaction saw low mass recovery as the system reached steady-state. All reported measurements were taken after a 90-minute equilibration period at which mass recovery exceeded 90%. To reach lower partial pressures of methyl lactate in this system, the inlet feed was at times diluted with 1,4-dioxane (99%, Sigma Aldrich). Control studies showed that no side reactions occurred between the dioxane and the Ti-containing zeolites at reaction conditions. Dioxane was selected as a diluent due to is ability to readily solubilize both methyl lactate and lactide while not overlapping any quantified peaks on the GC.

2.4 Results

2.4.1 Docking Simulations

As mentioned previously, docking simulations were carried out using lactide as a transition state proxy, with the computed binding energies as a function of framework shown in Figure 3 with the diameter of the largest sphere that can diffuse through the pore of the framework plotted on the x-axis. The commercial frameworks BEA and MFI (binding energies of -124 and -130 kJ/mol, respectively) were used as a benchmark for other frameworks. MEL was identified as a promising framework as it is well-studied, with many published synthesis recipes in the titanium form[59, 61-62] while also showing more favorable binding energies towards lactide (-134 kJ/mol). We hypothesized this more favorable binding energy would lead to higher selectivity of lactide employing a MEL zeolite catalyst compared to BEA or MFI.

Additional simulations were carried out docking other species from the scheme as well as significant side products such as the linear trimer. From these additional simulations, FER and TON stand out as additional frameworks of interest that were not able to be included in this study. FER was one of the only frameworks simulated with a negative energy change between the binding energy of the linear dimer and the binding energy of the lactide. This favorable energy change could allow Ti-FER catalysts to better convert the linear dimer to lactide. Additionally, there was no configuration in which the linear trimer was able to reside inside the FER channels. TON exhibits one of the lowest lactide binding energies of any zeolite screened, however it has 1-dimensional channels, which permit molecules to diffuse along only one dimension of the polymer. These FER and TON catalysts were not synthesized but remain candidates of interest (see Sec. 2.4 *Future Work*).

2.4.2 Catalyst Characterization

X-ray diffraction patterns of the synthesized MEL and MFI catalysts showed high crystallinity and purity via comparison to reference materials (Figures A-2 and A-3). Measurements from ICP-AES indicate these synthesized catalysts have Si/Ti ratio of ~150 whereas Ti-BEA-F has a lower site density (Si/Ti ratio ~300). Morphologically, MEL and MFI show structures according to SEM imaging that are similar to those found in literature for both zeolites, specifically cylindrical crystals with diameters of approximately 450 nm for MFI and larger, more irregular crystals for the MEL with diameters approaching 1 μm (Figures A-4 and A-5).

UV-Vis spectra for all three catalysts showed a strong absorbance peak at ~200 nm associated with tetrahedrally coordinated Ti that quickly decreased in the region of ~230-340 nm which would indicate presence of extra framework titanium oxide (Figure A-6). Due to the qualitative nature of UV-Vis spectroscopy, this cannot be used to determine the amount of tetrahedrally coordinated Ti present. Quantitative measurements would require infrared spectroscopic titration experiments as described in Johnson et. al.[63] However, the lack of absorbance in the region of titanium oxides indicates that our ICP-AES measurements should be a good representation of the number of active sites present in our catalysts.

2.4.3 Kinetic Studies

Initial results of gas-phase reactions for these catalysts are shown in Table 1. These reactions were run in the gas phase with a liquid feed flow of 0.1 mL min^{-1} of methyl lactate and 40 mL min^{-1} of N_2 carrier gas. Over a temperature range of 220-280°C, methyl lactate conversion was highest for the Ti-BEA-F catalyst despite the lower Ti content of this sample. While the lactide selectivity data was fairly noisy, there was no clear advantage of one catalyst over any other. Compositional analysis by GC revealed only two major side products, one which eluted before the lactide product and one which eluted after (Figure A-7). Analysis of these peaks through GC-MS revealed these compounds to be the methyl lactate dimer and trimer, respectively (Figure A-8). The more prominent peak, that of the dimer, is indicative of an incomplete reaction.

Table 1: Initial conversions and selectivities for the lactonization of methyl lactate to lactide as a function of temperature. All reactions were run with neat methyl lactate feed (0.15 mL min^{-1}) and ortho-xylene internal standard under N_2 flow (60 mL min^{-1}) and ~600 mg of catalyst with WHSV ~11 $g_{ML}\, g_{cat}^{-1}\, h^{-1}$

Catalyst	Temperature / °C	Methyl Lactate Conversion / %	Lactide Selectivity / %
Ti-BEA-F	230	20	31
	240	23	34
	250	25	38
	260	28	42
	270	31	46
	280	33	51
Ti-MFI-OH	220	7	51
	230	5	60
	240	10	39
	250	16	32
	260	22	30
	270	26	33
	280	29	38
Ti-MEL-OH	220	7	38
	230	8	41
	240	9	36
	250	15	34
	260	21	34
	270	27	46
	280	30	37

Comparing the methyl lactate conversion in Table 1 to De Clercq et. al.[57] at similar WHSV, temperatures, and pressure indicates these reactions were at significantly lower conversion and selectivity. To investigate this further, reaction effluent was collected from a standard reaction (250 °C, Ti-BEA catalyst) and fed back to the reactor at the same conditions in order to identify if the current reaction mixture had reached equilibrium. The relative intensity of the GC-FID peaks between the methyl lactate reactant and the internal standard remained constant pre- and post-reaction. Additionally, no additional lactide formation was detected. Therefore, we believe that under these conditions, the reaction had reached an equilibrium at approximately 25% methyl lactate conversion at 250 °C, despite previous literature experiments reaching 50% conversion at similar conditions. De Clercq et. al.[57] have shown that the equilibrium conversion and selectivities of this reaction depend on the gas phase concentration of methyl lactate, with lower concentrations yielding higher conversions and better lactide selectivities. Thus, further experiments diluted the methyl lactate feed (15 wt.%) in 1,4-dioxane with an internal standard (1 wt.% o-xylene). To maintain an appropriate WHSV, the catalyst bed was diluted in silicon carbide.

When comparing the two experiments at variable methyl lactate partial pressures at 250 °C and similar WHSV of ~15 h^{-1}, methyl lactate conversion increased from 30-50% to 55-75% and selectivity towards the desired lactide product increased from 30-45% to 60-75% when methyl lactate partial pressures were reduced. These increases are consistent with the effects of methyl lactate concentration in the gas stream shown in De Clecq et. al.[64] further work used this dilute condition to maintain better parity with literature.

A comparison study of the three frameworks of interest, Ti-MFI-OH, Ti-MEL-OH, and Ti-BEA-F is shown as a function of time-on-stream at 250 °C and WHSV of ~15 h^{-1} in Figure 4. Following the first 4 samples on Ti-MEL-OH, the WHSV was increased to ~20 h^{-1} by increasing both the feed mixture flow rate and nitrogen flow rate, keeping the gas phase composition identical. This was done to decrease the conversion over Ti-MEL-OH to better match that of the other two catalysts. At WHSV ~15 h^{-1}, significantly higher methyl lactate conversion was observed over the Ti-MEL-OH catalyst compared to Ti-BEA-F and Ti-MFI-OH. Additionally, Ti-MEL-OH produces much less of the (incompletely reacted) linear dimer. This decrease in dimer concentration may be the result of thermodynamically favorable interactions encouraging cyclization provided uniquely by the MEL framework. Interestingly, there was a larger presence of the linear trimer in the Ti-MEL-OH products, which may be attributable to the linear channels of the zeolite framework permitting longer, linear structures as opposed to the sinusoidal channels of MFI. At comparable conversion, Ti-MEL-OH maintains its improved selectivity over the other frameworks, indicating this effect is not an artifact of high conversion. Together, these results suggest the specifically-selected MEL displays improved performance over generic frameworks.

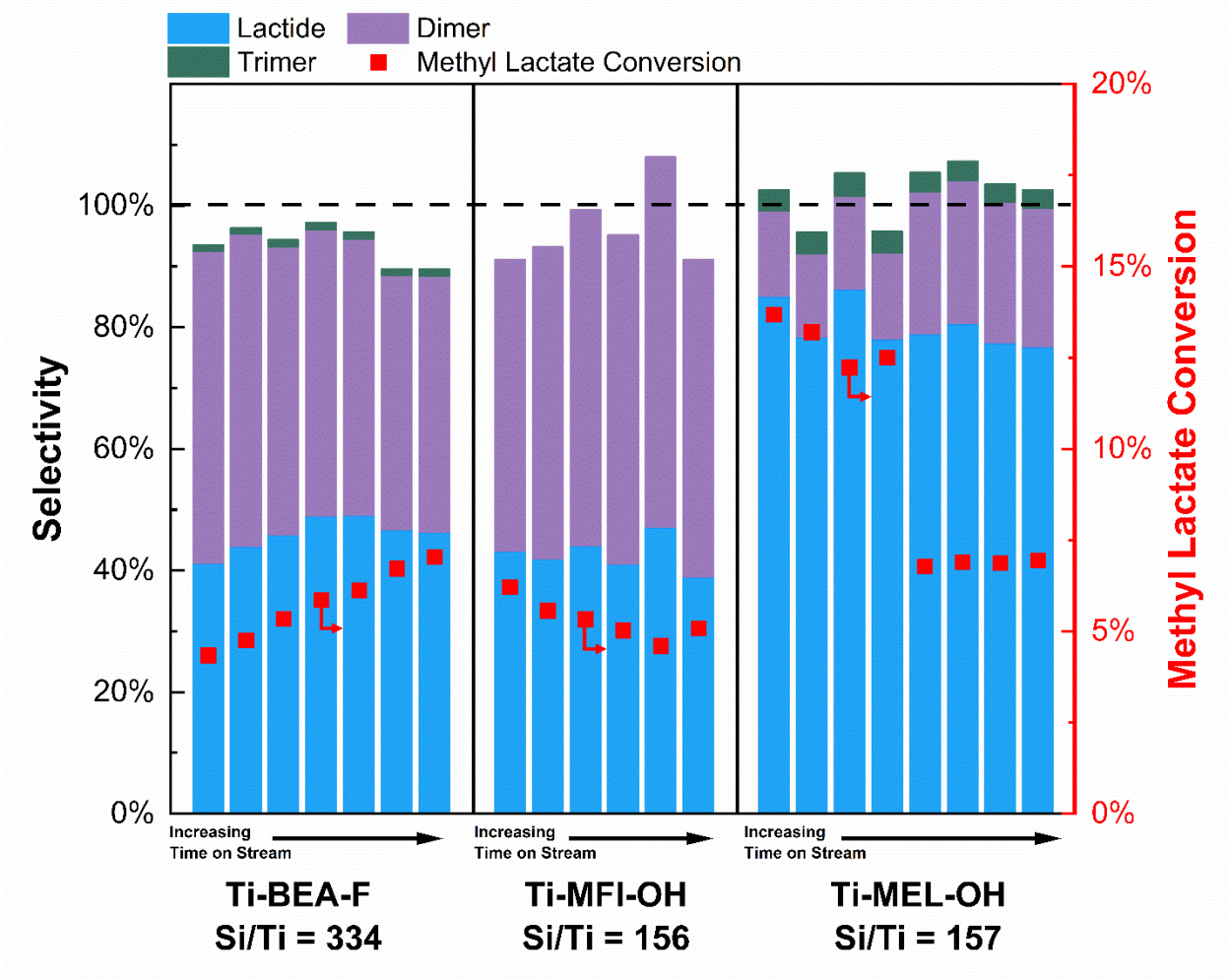

Figure 4: Comparison of different zeolite frameworks (~100 mg) for the production of lactide at 250 °C and a WSHV of 15 $g_{ML}\,g_{cat}^{-1}\,h^{-1}$. Feed was 15 wt. % methyl lactate, 1 wt. % o-xylene, and balance dioxane at 0.15 mL min^{-1} to reach a WSHV of 15 $g_{ML}\,g_{cat}^{-1}\,h^{-1}$. Each vertical bar represents a different sample taken approximately 20 min apart. Ti-MEL-OH was first run at a WHSV of 15 $g_{ML}\,g_{cat}^{-1}\,h^{-1}$ before increasing to 20 $g_{ML}\,g_{cat}^{-1}\,h^{-1}$ for the fifth data point and beyond.

Additional studies were conducted to further probe the lactonization reaction pathway outlines in Scheme 1. First, a large amount of reactor effluent was collected following 4 days of 8-hour reactions over Ti-MFI-OH (methyl lactate conversion ~5%). This partially-reacted mixture was fed back into the reactor in multiple experiments over various catalysts. The details of these experiments are shown in Table 2. First, the second pass behavior over both Ti-MFI-OH and Ti-MEL-OH was examined. The Ti-MFI-OH resulted in an increase in the methyl lactate conversion from 5% to 8% and an increase in the lactide selectivity from about 45% to about 63%. Estimating the dimer production in both showed a slight increase in the molar flow of the dimer after the recycle. Recycle over Ti-MEL-OH also showed increases in both conversion and selectivity, though the increases were significantly larger. The recycle over MEL resulted in a methyl lactate conversion of 13% and a lactide selectivity of 80%. Additionally, we saw that the molar flowrate of the linear dimer out of the reactor actually decreased slightly despite the large increase in lactide production and methyl lactate consumption, indicating that the MEL framework may favorable catalyst this second reaction step.

Table 2: Feed recycle study over Ti-MFI-OH, Ti-MEL-OH, and De-Al-BEA. First pass feed was comprised of 15 wt. % methyl lactate, 1 wt. % o-xylene, and balance dioxane. WHSV for titanium-containing zeolites during both passes were 15 $g_{ML}\,g_{cat}^{-1}\,h^{-1}$ (feed flow rate of 0.15 mL min^{-1} and ~100 mg catalyst).
** Reactions for De-Al-BEA were run at one-half the WHSV of 6 $g_{ML}\,g_{cat}^{-1}\,h^{-1}$ by increasing catalyst loading to 260 mg.*

Molar Flow Rates	1st Pass over Ti-MFI-OH	2nd Pass over Ti-MFI-OH	2nd Pass over Ti-MEL-OH	2nd Pass over De-Al-BEA*
Methyl Lactate Conversion	5%	8%	14%	8%
Lactide Selectivity	45%	63%	80%	39%
$\dot{n}_{\text{Methyl Lactate}}$(mmol h^{-1})	13.62	13.17	12.41	13.19
$\dot{n}_{\text{Dimer}}$(mmol h^{-1})	0.14	0.16	0.12	0.07
$\dot{n}_{\text{Lactide}}$(mmol h^{-1})	0.16	0.36	0.77	0.22
$\Delta\dot{n}_{\text{Methyl Lactate}}$(mmol h^{-1})	0	-0.45	-1.21	-0.43
$\Delta\dot{n}_{\text{Dimer}}$(mmol h^{-1})	0	0.02	-0.02	-0.07
$\Delta\dot{n}_{\text{Lactide}}$(mmol h^{-1})	0	0.2	0.61	0.06

An additional test was performed using de-aluminated commercial BEA catalyst. This provided a catalyst with a significant concentration of silanol nests due to the removed aluminum. Being mildly acidic and also capable of changing local pore environments, it was necessary to determine if silanol nests could be responsible for the reactivity trends seen in the previous studies, especially the hydrophilic MEL and MFI frameworks. Tests with this catalyst were performed at half the WHSV (~6 h^{-1}) as reactivity was expected to be very small. Running the reaction with de-aluminated BEA and a fresh feed resulted in a methyl lactate conversion of ~2% with low selectivity to lactide (~9%). Running partially converted feed over this catalyst (5% methyl lactate conversion), resulted in an increase in the methyl lactate conversion similar to that of the Ti-MFI-OH at a WHSV of 15 h^{-1} and a slight increase in the lactide molar flow (Table 2), though the selectivity towards lactide fell. This indicates that the silanol groups in the framework can have effects on this reaction and further study and quantification of these sites is necessary to fully understand this system. This dealuminated catalysts represents the upper extreme of silanol density, so the expected contribution of the silanol nests in the other reactions is small relative to the effect of the framework.

With these studies of the gas-phase dimerization and subsequent lactonization of methyl lactate over titanium-containing zeolite catalysts, we were able to show an increase in the selectivity towards the desired product through the selection of a framework our simulations predicted would more favorably bind our product. This Increase in selectivity over Ti-MEL-OH was accompanied by an increase in methyl lactate conversion when compared to similar Ti-MFI-OH catalysts.

2.5 Future Work – Gas Phase Lactonization Study

While this initial study was promising, there are multiple outstanding questions that could be addressed by future studies. Firstly, this reaction was performed in the gas phase to avoid solvation effects, and it is thus expected that the differences between hydrophilic and hydrophobic frameworks are minimal. However, this is an important control to further strengthen the claim of favorable binding interactions. Ideally, three additional catalysts would be synthesized: fluoride-media synthesized hydrophobic Ti-MFI-F and Ti-MEL-F, to compare to their hydrophilic counterparts, and Ti-BEA-OH, produced by Ti-grafting into de-aluminated BEA, to compare to Ti-BEA-F. Comparing these three catalysts at identical conditions as well as at isoconversion would discern if MEL performs better due to its hydrophobicity or the strength of its thermodynamic interactions. If hydrophobicity is indeed important to these gas phase reactions, that is an interesting property of the catalyst worthwhile of future study.

Secondly, the three zeolite frameworks selected for this study were chosen based only on the binding energies of the lactide product due to the endothermic nature of this reaction. However, this may not be the optimal method for framework selection if, for example, all species' binding energies were lowered by a

roughly equal amount by a framework. This complete shift of the free energy diagram of this reaction would produce no significant change in the selectivity. Additionally, we might have not selected a certain zeolite due to relatively high lactide binding energy despite the fact that this state is significantly more favorable than the dimer binding energy, more so than some of the frameworks we tested here. From the additional simulations mentioned earlier, FER and TON remain viable candidates for further improvement of performance. The data for all aluminum-containing zeolite frameworks with medium or larger pores are shown in Figures A-9 to A-12, and a down selection to five zeolite frameworks is shown in Figure 5. As kinetic studies revealed that the linear dimer is the most prominent side product, the potential ability of FER to accelerate its conversion could be very impactful on the overall reaction. However, care should be taken in using TON as its 1-dimensional channels may be more affected by deactivation from trimer or oligomer formation.

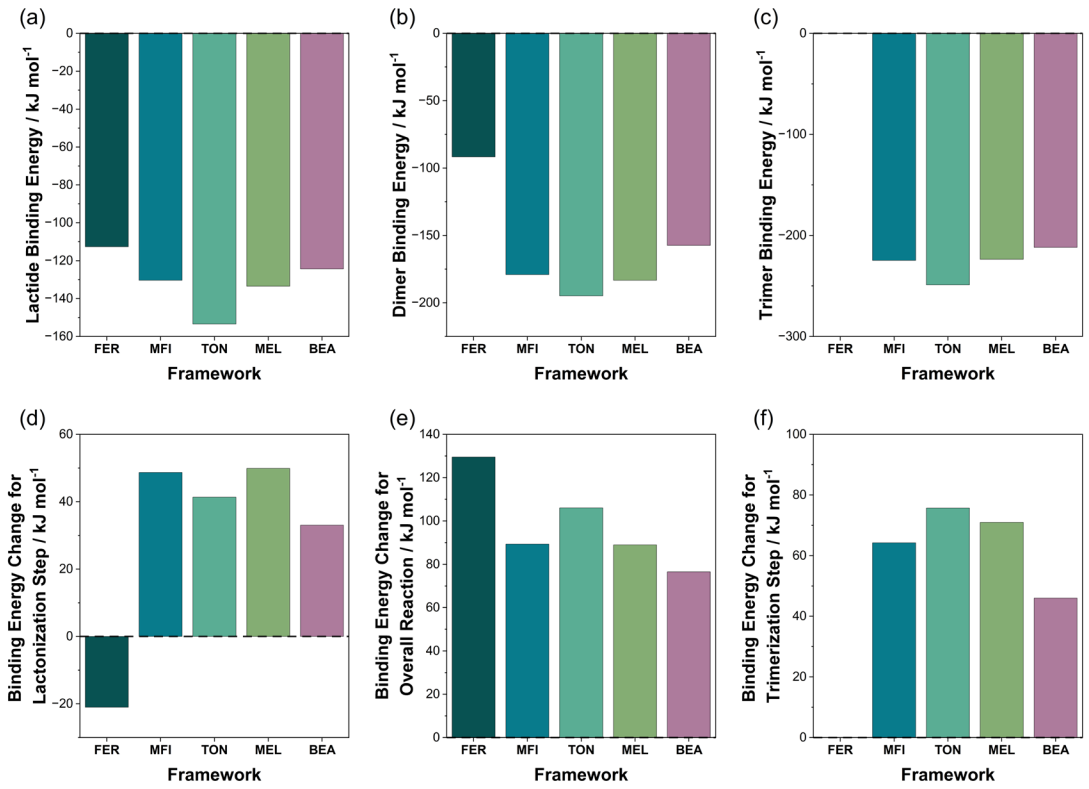

Figure 5: Data from additional docking simulations. a) Shows Lactide binding energies. b) Shows Dimer Binding Energies c) Shows trimer binding energies (docking not possible for FER). d) Shows the change in binding energy for the lactonization step (Dimer to Lactide in Scheme 1). e) Shows the change in binding energy for the overall reaction (e.g., binding energy of lactide – twice the binding energy of methyl lactate). f) Shows the change in binding energy for the trimerization step (Dimer to Trimer in Scheme 1)

3. Developing New Pathways to CVL Monomers

3.1 Executive Summary

In this study we have shown the successful engineering of a flow reactor capable of producing α-methylene-δ-valerolactone (MVL) at high selectivity and moderate conversion through the aldol condensation of δ-valerolactone (DVL) and formaldehyde over solid Lewis base catalysts. Further experiments starting from the MVL molecule showed further functionalization through the Diels-Alder addition of 1,4-butadiene and subsequent hydrogenation to form the cyclohexyl-substituted lactone (CVL) at high selectivity albeit over long reaction times using Lewis acidic zeolite catalysts. Both MVL and CVL are desirable monomers for next generation intrinsically recyclable plastics.

3.2 Approach

Previous studies have shown that the continuous aldol condensation of γ-valerolactone (GVL) with formaldehyde to form α-methylene-γ-valerolactone (MGVL) over barium oxide supported on silica.[65] This study showed >95% selectivity to MGVL at 613 K. Using this work as a starting point, a continuous-flow system was constructed for the aldol condensation of δ-valerolactone (DVL) and formaldehyde using silica-supported alkaline earth oxide catalysts (Scheme 2).

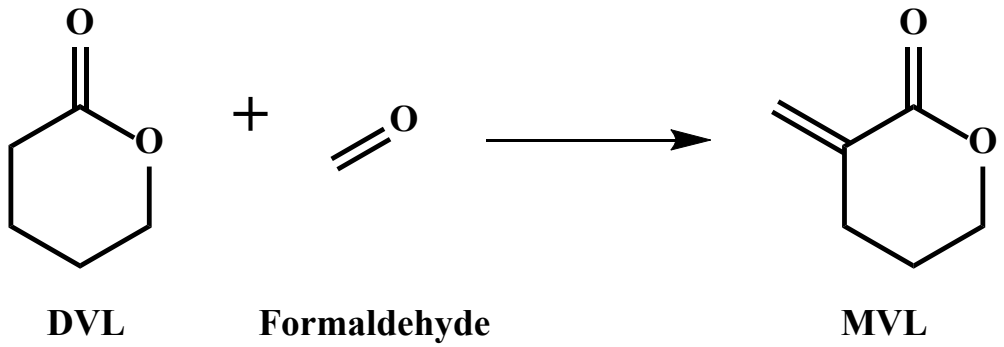

Scheme 2: Aldol Condensation of DVL and Formaldehyde

Following the synthesis of MVL in a continuous-flow reactor, further functionalization towards CVL was desired as depicted in Scheme 3. To achieve this, the route of Diels-Alder addition was pursued, as there is a wealth of literature on this reaction over heterogeneous catalysts.[66] Common catalysts for Diels-Alder are substituted zeolites, mesoporous aluminosilicates, and metal oxides.[66] Similar to zeolites, MCM-41 is a material with tetrahedrally coordinated silica. However, the lack of a well-defined crystal structure gives rise to much higher hydrophilicity and mesopores, allowing for the uptake of molecules larger than what is allowed for zeolites without post-synthetic modifications.

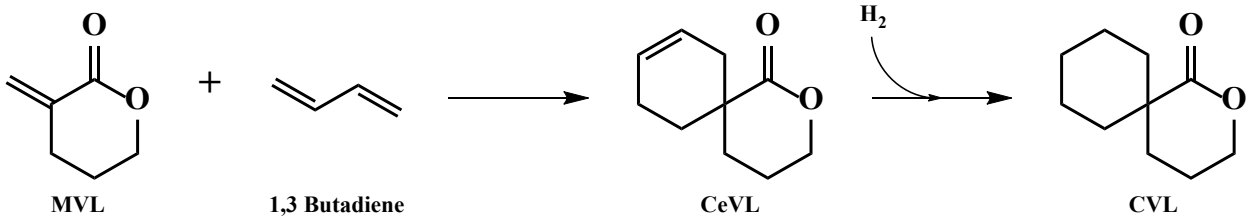

Scheme 3: Diels-Alder addition of 1,3-butadiene to MVL followed by hydrogenation to form CVL

3.3 Methods

3.3.1 Catalyst Synthesis

All metal oxide catalysts supported on silica were prepared via incipient wetness impregnation. Fumed silica (SiO_2, Sigma Aldrich) that had previously been calcined at 550 °C for 6 h was used as the support. Synthesis of the alkaline earth oxide catalysts used in the MVL synthesis used the acetate form of the metal: magnesium acetate tetrahydrate, calcium acetate monohydrate, or barium acetate (all >99%, Sigma Aldrich). For tin oxide, tin (IV) chloride pentahydrate (98%, Sigma Aldrich) was used as the metal source. In all cases, the metal source was dissolved in enough Milli-Q water to saturate the pore volume of a given mass of SiO_2 (~2 $g_{water}\, g_{SiO2}^{-1}$). The metal salt solution was then added dropwise to the silica followed by grinding and mixing in a mortar and pestle. The silica-metal pre-catalyst was dried overnight at 100 °C overnight followed by an additional grinding step and calcination to 500 °C for 6 h.

The Hf-BEA-OH catalyst was synthesized by previous lab members and detailed in Khechfe et. al.[67] De-aluminated BEA (synthesized as in Section 2.2.1) was added to a 500 mL two-neck flask with a magnetic stir bar. The catalyst was dried under vacuum conditions and heated to 350 °C overnight to remove water in the pores. Once the material had cooled to room temperature and the vessel was filled with nitrogen, 130 mL of acetonitrile (HPLC grade, Sigma Aldrich) was added while stirring. An amount of hafnium (IV) chloride (98%, Sigma Aldrich) depending on the desired concentration of Hf sites was dissolved in 10 mL of acetonitrile and added to the flask. This mixture was then refluxed at 85 °C overnight to incorporate the Hf. The catalyst was calcined in flowing air at 580 °C for 6 hours.

Hydrophobic metal containing BEA zeolites (Hf, Sn, Zr, Ti) were synthesized by prior members of the lab following procedures outlined in Camblor et. al.[58] For non-Sn containing zeolites, metal precursors were replaced with the appropriate metal chloride hydrates. New zeolite materials were not synthesized for this project.

Sn-MCM-41 catalyst was synthesized by prior members of the lab as described in Luo et. al.[68]

Scandium Triflate, $Sc(SO_3CF_3)_3$ supported on silica was prepared following the procedure described in Chen et. al.[69] Approximately 1 g of fumed silica (SiO_2, Sigma Aldrich) which has been previously calcined at 550 °C for 6 h was added to 50 mL of ethanol (200 proof, Koptec)) and 0.50 g of scandium triflate (99%, Sigma Aldrich). This mixture was allowed to react under vigorous mixing with a PTFE-lined magnetic stir bar at 60 °C for 24 h. Following the reaction, the material was washed with ethanol to remove any uncoordinated scandium triflate.

3.3.2 Catalyst Characterization

Weight loadings of Mg, Ca, and Ba on SiO_2 were determined by inductively coupled plasma mass spectrometry (ICP-MS) using an Agilent 7900 ICP-MS instrument. Approximately 10 mg of catalyst powder was added to a 15 mL polypropylene centrifuge tube and dissolved in ~1 mL of 68.0% HNO_3 (Veritas double distilled, GFS Chemicals Inc.) overnight, followed by dilution in 2 wt. % HNO_3 and filtration through a 0.2 μm PTFE syringe filter (VWR) to remove the undissolved SiO_2 support. Solutions were further diluted to obtain metal concentrations of 100-300 ppb for Mg, and Ba. Ca solutions were diluted to a lesser extent (30-60 ppm) to monitor ^{44}Ca (~2% abundance) due to interference between ^{40}Ca and the Ar plasma. Metal concentrations were determined from calibration curves prepared from standard solutions of 1000 ppm of Mg, Ca, and Ba (all TraceCERT, Sigma-Aldrich), diluted in 2 wt. % HNO_3.

Weight loadings for Sn-MCM-41, Hf-BEA-F, Ti-BEA-F, Sn-BEA-F, and Zr-BEA-F were calculated via ICP-MS by previous members of the group as described in Wang et. al.[70] and Luo et. al.[68]

Carbon dioxide temperature programmed desorption (CO_2 TPD) was performed in a Micromeritics Autochem II 2920 unit equipped with a thermal conductivity detector. Approximately 0.15 g of sample was loaded into a quartz U-tube and held in place with plugs of quartz wool on both sides. The sample was pretreated in 50 mL min^{-1} He at 473 K for 2 h and then cooled to 313 K. The sample was then dosed with 50 mL min^{-1} of a 1% CO_2 in N_2 mixture along with 30 mL min^{-1} He for 30 min, followed by a 10 min purge in 80 mL min^{-1} of He. This procedure was repeated an additional two times to saturate the surface with CO_2. The sample was then heated in 80 mL min^{-1} He flow while the temperature was ramped from 313 K to 1073 K at a 10 K min^{-1} ramp rate while monitoring the reactor effluent.

Thermogravimetric analysis (TGA) was performed on a TA Instruments Q500 System. The sample was loaded onto a tared platinum pan and equilibrated at 298 K in 45 mL min^{-1} of air and 5 mL min^{-1} N_2. After equilibration, the temperature was ramped at 1 K min^{-1} to 1073 K.

3.3.3 Chemical Quantification

Reaction products were quantified using an Agilent 8890 Gas Chromatography Unit with a HP-5ms Ultra Inert column (30 m x 250 μm x 0.25 μm). Varying flow rates of a known mixture of formalin (37 wt. % FA in water with methanol stabilizer, Sigma Aldrich), DVL (technical grade, Sigma Aldrich), and MVL (provided by the Chen group from Colorado State University) were sent through a bypass route of the reactor to the online GC to create calibration curves. Standard solutions of para-xylene (98%, Sigma Aldrich), 1,3-butadiene (20 wt. % in toluene, TCI) and MVL in toluene (99.8%, Sigma Aldrich) were prepared to create standards relative to para-xylene. CeVL standards were created following the same method after separating it out of the reaction products through flash chromatography and evaporation. Quantity of CeVL was determined though Hydrogen Nuclear Magnetic Residence (H-NMR) with para-xylene external standard.

CeVL and CVL were identified using ^{1}H-NMR, ^{13}C-NMR, and Heteronuclear Single Quantum Coherence (HSQC) performed on a Bruker Avance Neo spectrometer operating at 500.34 MHz. Chemicals were diluted in chloroform-d (99.8 atom % D, Sigma Aldrich) for analysis.

3.3.4 Reactor Configuration(s) and Procedure

Aldol condensation between DVL and formaldehyde (FA) were performed in a gas-phase, fixed bed reactor constructed from Swagelok fittings and 316 stainless-steel tubing sourced from McMaster-Carr. A mixture of DVL and formalin were introduced via a Cole-Parmer Masterflex Single-Syringe Infusion Pump with a typical liquid flow rate of ~0.16 mL h^{-1}. The liquid feed was vaporized at ~423 K into a stream of hot N_2

(UHP, Airgas) with a typical flow rate of 50 mL min^{-1} supplied by a Brooks GF40 Series mass flow controller. All reactor lines were heated with heating tape (BriskHeat) and insulation using a VARIAC (Automation Technology, 2KW) and external K-type thermocouples to maintain gas-phase flow during operation. The reactor (1/4" O.D., 316 stainless steel tube) was kept isothermal inside a furnace (Applied Test Systems) and controlled by a K-type thermocouple touching the base of the catalyst bed attached to a temperature controller (Cole-Parmer Digi-Sense R/S 68900-11). Inside the reactor, the catalyst bed consisted of ~0.1 g crushed, sieved catalyst (40-60 mesh) mixed and diluted with ~0.4 g SiC (46 mesh), trapped between plugs of quartz wool and topped with ~1.5 g of borosilicate glass beads to facilitate gas-phase mixing. Reactor effluent was analyzed by an on-line gas chromatograph (Agilent 8890) equipped with a 30 m HP-5MS-UI column with FID. Product selectivities are calculated as $S_i = 100\% \times \dot{n}_i / \left(\dot{n}_{DVL,o} - \dot{n}_{DVL}\right)$ where S_i is the selectivity of product i, $\dot{n}_{DVL,0}$ is the initial molar flow rate of DVL into the reactor, and $\dot{n}_{DVL}$ and $\dot{n}_\iota$ are the molar flow rates of DVL and product i in the effluent, respectively. Contact times are calculated as moles of active metal loaded in the reactor divided by the molar flow rate of DVL ($mol_{metal}\ mol_{DVL}^{-1}\ h^{-1}$).

Batch reaction experiments for the production of cyclohexene-substituted δ-valerolactone (CeVL) were performed in glass reactors with crimped-top PTFE septa. Typically, 200 μL of MVL 50 μL para-xylene internal standard, and 2 mL 20 wt. % 1,3-butadiene in toluene solution were added along with a PTFE-lined magnetic stir bar. To this mixture, approximately 100 mg of catalyst was added, after which the vial was sealed and allowed to react under vigorous stirring at ambient temperature. Liquids were then removed and filtered from the catalyst for analysis. Temperature studies were performed by immersing the reaction vials in a pre-heated silicone bath at the reaction start and quenching them in ice for sampling. Once cold, aliquots were sampled by removing the top, sampling, and replacing, to avoid puncturing the PTFE and therefore causing butadiene losses at temperature. After sampling events, all vials were returned to the bath simultaneously.

Water-free reactions over highly hydrophilic catalysts such as MCM-41 were performed as follows. The catalyst was heated under vacuum at 200 °C overnight in a two-neck round-bottom flask with an FKM septum on one neck and vacuum line on the other. Dry nitrogen was then introduced to the catalyst and the liquid components were added vial syringe through a septum on the reaction vessel. Additionally, the reaction mixture was dried with 4Å molecular sieve overnight to remove water present in the reactants. GC analysis after drying but before the introduction to the catalyst showed no reaction with these sieves.

The hydrogenation of CeVL to CVL was performed in a round bottom flask to which approximately 1 mmol of CeVL, 18 mg of commercial Pd/C (Sigma Aldrich) and 100 mL of Hexanes (Macron Chemical) were loaded. Hydrogen (UHP, Linde) was fed at 10 mL min^{-1} into the reactor via a 1/8" O.D. 316 stainless steel tube to bubble through the liquid mixture. This mixture was stirred and heated to 50 °C overnight. The liquid was collected and filtered with a 0.2 μm PTFE syringe filter and solvent was then removed via evaporation.

3.4 Catalyst Screening for the Gas-Phase Production of MVL

3.4.1 Catalyst Characterization

The metal loadings of the catalysts were identified with ICP-MS and the resulting metal loadings of the metal oxides supported on silica are shown below in Table 3, while the Si/M ratios for the zeolites and other catalysts used for the CeVL production study are including in Table 3.

Table 3: Weight loadings of metal oxides on silica

Catalyst	Metal Weight Loading
MgO/Silica	3.6%
CaO/Silica	5.2%
BaO/Silca	3.9%

CO_2 TPD showed both CaO and BaO catalysts with desorption features at temperatures greater than 600 K. The MgO catalysts, conversely, showed desorption features only in the region below 600 K, indicating weaker basic sites than the CaO and BaO catalysts (Figure A-13).

The metal oxide catalysts were also studied post-reaction via TGA (Figure A-14). After approximately 6 to 8 hours of time on stream, the catalysts were removed and heated to 1073 K in flowing air. All catalysts showed some mass loss at around 400 K which is hypothesized to correspond to non-coke surface species. This includes lactone dimers and other heavy molecules that may not desorb from the catalyst during normal operation, but are not truly coke deposits (see Figure A-15 for possible reaction pathways). MgO showed additional mass loss up to around 700 K indicating the presence of coke deposits on this catalyst.

3.4.2 Catalyst Screening for the Gas-Phase Production of MVL

Initial trials were carried out with a partial pressure of 0.4 kPa DVL and 1.2 kPa formaldehyde (formed by thermal decomposition of formalin) during which primarily, the formation of the desired MVL product was observed, and subsequently confirmed using ^{1}H-NMR. Other side products for all reactions included α-methyl-δ-valerolactone and GVL. Each catalyst was additionally tested over a range of contact times (Figure 6), showing at low contact times high selectivities towards the desired MVL product, though with low conversions. At higher contact times, more of the DVL feed became lost carbon, unaccounted for in the GC-FID analysis of the outlet gas. Across the three catalysts, MgO and BaO generally produced higher conversions than CaO, but MgO tended to yield a worse carbon balance than CaO or BaO. This difference may be attributable to the stronger basic sites on BaO and CaO, as shown through these catalysts' higher desorption temperature in CO_2 TPD. CaO featured 90% MVL selectivity at 60% DVL conversion at a contact time of 0.6 h.

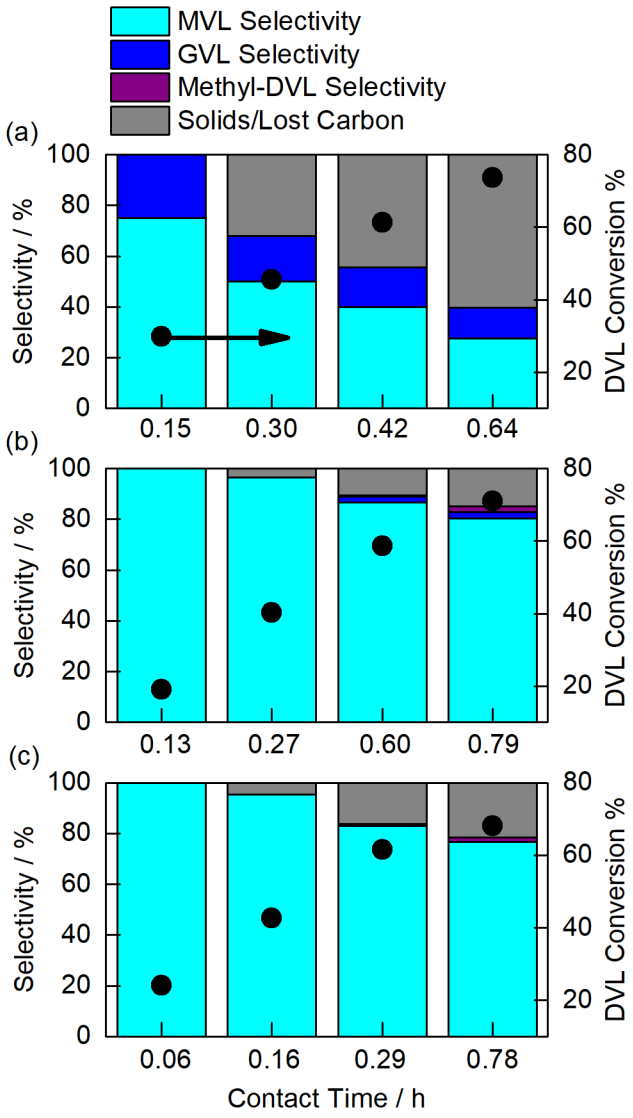

Figure 6: Product distributions and DVL conversions as functions of contact time for (a) MgO/SiO_2, (b) CaO/SiO_2 and (c) BaO/SiO_2 (613 K, 0.1 g catalyst, 0.4 kPa DVL, 1.2 kPa FA, 101 kPa total pressure with balance N_2).

3.4.3 Catalyst Screening for Conversion of MVL to CeVL

A variety of heterogenous Lewis acid catalysts, including zeolites, mesoporous materials, and bulk metal oxides were screened to identify promising candidates for CeVL production compared with a benchmarking homogeneous $SnCl_2$ dihydrate (99.995% trace metals basis, Sigma Aldrich). The catalyst compositions, silicon to metal ratios, and site-normalized rates are reported in Table 4. To account for the difference in active sites, a similar molar amount of tin was added for $SnCl_2$ study as with respect to Sn-BEA.

Table 4: Si:M ratios and TOF for the production of CeVL over various catalysts. All reactions run in sealed glass reactor vials under constant stirring at ambient temperature. Reactor vials contained 200 μL MVL, 50 μL p-xylene, and 2 mL of 20 wt. % 1,3-butadiene in toluene. Approximately 50 mg of sample were added for all heterogeneous catalysts. An equivalent about of Sn to the Sn-BEA-F experiment was added for the $SnCl_2$ experiment, rather than 50 mg. Reactions were run overnight.
**These reactions were run under water-free conditions as described in section 3.3.4*

Catalyst	Si : M	TOF (mol_{CVL} mol_M^{-1} h^{-1})
$SnCl_2$	N/A	0.49
Hf-BEA-F	197 : 1	0.70
Sn-BEA-F	106 : 1	0.60
Zr-BEA-F	104 : 1	0.06
Ti-BEA-F	109 : 1	0.30
Al-MCM-41*	12.5 : 1	0.03
Sn-MCM-41*	115 : 1	0.09
Hf-BEA-F*	197 : 1	0.42
Hf-BEA-OH*	145 : 1	0.07
ScTriflate/SiO_2	~17 : 1	0.04
Nb_2O_5	N/A	~0
SnO/SiO_2	~20 : 1	~0

The homogeneous $SnCl_2$ produced a site normalized rate of 0.49 h^{-1}, indicating that this reaction proceeds quite slowly. Similar, though lower, rates are observed for Hf-BEA and Sn-BEA, while Ti-BEA and Zr-BEA were significantly slower. Achieving high conversions is therefore difficult. The reaction does not appear to be equilibrium-limited, as the conversion-time trend remains linear up to ~40% (Figure A-16) and the expected equilibrium is ~100% based on computations for Diels-Alder additions and our low temperatures pushing equilibrium formward.[71] Increasing metal loading is difficult as larger atoms like Sn and Hf place strain on the zeolite framework and easily lead to extra-framework oxides at high metal concentrations which may act very catalytically different. While it is possible to achieve high Sn loading, it is most often accomplished through dealumination procedures to obtain hydrophilic frameworks.[72] The feasibility of metal oxide-catalyzed conversion was tested with SnO_2 supported on silica. After 48 hours at ambient temperature, no CeVL yield or MVL conversion was detected. Additional tests were performed with other Lewis acidic catalysts in the form of Nb_2O_5 powder (99.99% trace metal basis, Sigma Aldrich) and Scandium Triflate, $Sc(SO_3CF_3)_3$, supported on silica. Both alternative catalysts showed very small yields of CeVL, with much slower site-normalized rates than that of the Lewis acidic zeolites. The mesoporous Al-MCM-41 (ACS Materials, MSM41B) and Sn-MCM-41, tested water-free, were also an order of magnitude slower than that of the hydrophilic Hf-BEA. A follow up experiment to further probe the effects of the hydrophobicity of the framework was performed with two different Hf-BEA samples. The first was the same catalyst used in previous studies, directly synthesized in fluoride media to minimize the amount of silanol nests. Both of these catalysts were tested under water-free conditions and showed that

the hydrophobic sample had a CeVL production rate ~10-fold higher than that of the hydrophilic BEA. Additionally, air- and water-free conditions resulted in a slightly lower rate than ambient conditions, indicating that a small presence of water may be beneficial for this reaction.

In an effort to increase the rate of reaction, Sn-BEA-F and Ti-BEA-F were selected for examining the effects of temperature, Sn-BEA-F as a high-performing catalyst and Ti-BEA-F to provide a contrast. Over the approximately 90-hour experiment, the final MVL conversion over Sn-BEA increased from 42% to 75% and the selectivity towards CeVL increased from 52% to 90% (Table 5). Analysis by GC-FID was unable to identify any peaks that could be responsible for the missing carbon in these reactions. Similarly, there was an increase in both the MVL conversion and CeVL selectivity for the Ti-BEA catalyst, though the final selectivity plateaus around 60%. While there was some reactivity in the trials performed in the absence of catalyst, it is not enough to explain the increase in conversion and selectivity.

Table 5: Temperature study of CeVL reaction. Each reaction vial was loaded with 100 mg of catalyst, if present, 200 µL of MVL, 100 µL of p-xylene, 2 mL of 20 wt. % 1,3-butadiene in toluene, and a magnetic stir bar. The reaction was allowed to proceed for 86 h with samples taken at 11, 18, and 45 h with the method described in section 3.3.4. Final MVL conversions and CeVL selectivity were calculated from the final time point.

Catalyst	Temperature / °C	Final MVL Conversion / %	Final CeVL Selectivity
Sn-BEA-F	25	42	52
	40	63	70
	55	75	90
Ti-BEA-F	25	25	43
	40	46	60
	55	68	59
No Catalyst	25	0	N/A
	40	~0	N/A
	55	7	91

3.4.4 Conversion of CeVL to CVL

The previous studies were done under the assumption that the final step of Scheme 3, the hydrogenation of CeVL to CVL, would be simple and almost perfectly selective. Testing this required the collection of all post-reaction solutions of the temperature study in order to collect enough CeVL to attempt hydrogenation. The CeVL was separated from the reaction mixture using a Biotage Selekt flash chromatography unit with Silica column. A 50:50 mixture of hexane and ethyl acetate was used to separate the CeVL from the other reaction components. The hexane and ethyl acetate were removed by evaporation and the resulting liquid was analyzed with ^{1}H-NMR, ^{13}C-NMR, and HSQC (Figures A-17 to A-19). Though some impurities were present, we were able to confirm that this was CeVL due to hydrogen peaks around 5.4 ppm corresponding with the alkene bond on the second ring. Following this reaction, the CVL product was isolated via evaporation and NMR was once again performed. The new NMR spectra showed no peaks in the alkene region as shown in Figure A-20. This indicates that, indeed, the hydrogenation of the unsaturated bond of CeVL is able to be done in a single step and mild conditions with commercially available catalyst.

This study has shown the continuous, gas-phase synthesis of MVL, functionalization to CeVL, and hydrogenation to the target molecule of CVL. Catalyst screening revealed that CaO on silica was the best catalyst for the aldol condensation of DVL and formaldehyde leading to nearly 100% selectivity towards the desired product even at relatively high conversions of 40%. Following this study, we showed that this

MVL could be functionalized with a second ring through the Diels-Alder addition of 1,3-butadiene. This reaction, while slow, proceeded over Lewis-acidic zeolites containing tin and hafnium. Increasing the temperature of the reaction from room temperature to 50 °C on Sn-BEA-F zeolites increased the selectivity to 90% at conversions of 75%. Finally, this CeVL was separated from the solvent and reactants and hydrogenated over commercial Pd/C catalyst to near complete conversion overnight at mild conditions.

3.5 Future Work - DVL to CVL Pathway Optimization

Further optimization of the first step of this process may be possible through the engineering of catalysts to reduce the formation of lactone dimers that lead to catalyst deactivations. This could potentially be achieved through the confinement of the active sites in porous materials with pores too small to accommodate lactone dimers. Additional MVL reactor scale-up and product collection methodologies would allow for an increased scale of in-lab MVL production, avoiding complex organic chemistries[73] and facilitating larger-scale studies with MVL as a reactant. This would also require separation techniques to isolate the MVL from the DVL or the ability to recycle the reaction stream until full conversion is reached.

The production of CeVL shown here has been promising, but the slow reaction rate and batch-phase reactions limit the amount of CeVL (and thus CVL) that can be produced. Future studies on the polymerization of CVL and subsequent recycling must be conducted to complete the pathway from biomass derivatives to desirable polymer. In order to collect sufficient CVL to perform polymerization and recycling studies, yields must be improved. Other forms of porous catalysts may result in higher activity for this reaction. Previous studies have shown that hexagonal mesoporous silica (HMS) gives increased reaction rates for Diels-Alder reactions when compared to MCM-41 and zeolites.[74] Following additional catalyst optimization, it would be preferential to convert this reaction to a continuous-flow process to further increase throughput. Currently, slow reaction rate over these catalysts prevents running in the continuous phase, due to necessary low flow rates or high catalyst loadings. Once a better catalyst has been found, these efforts may become more promising. Finally, optimization of the hydrogenation step should be conducted, as the experiment shown here was merely a proof-of-concept to show hydrogenation was possible.

4. Conclusion

In this work, we have shown the viability of using high-throughput computational screens to select zeolite frameworks to selectively catalyze a reaction of interest resulting in significantly higher selectivities than other catalysts previously studied in literature. Future studies involving the expansion of these simulations to include more docked species have been proposed. Additionally, we have shown a potential pathway for the production of α-cyclohexyl-δ-valerolactone (CVL). The first step in this process is the aldol condensation of formaldehyde and δ-valerolactone (DVL) over alkaline earth oxides supported on silica in a gas-phase continuous reactor to form α-methylene-δ-valerolactone (MVL). Following this, MVL was functionalized over Lewis acid catalysts at mild conditions through the Diels Alder addition of 1,3-butadiene. Finally, this unsaturated product was hydrogenated to form the desired CVL using commercially available Pd/C catalyst.

5. Acknowledgements

The methyl lactate study was performed as part of the Bio-Optimized Technologies to keep Thermoplastics out of Landfills and the Environment (BOTTLE) Consortium and was supported by AMO and BETO under Contract DE-AC3608GO28308 with the National Renewable Energy Laboratory (NREL), operated by Alliance for Sustainable Energy, LLC. The BOTTLE Consortium includes members from MIT, funded under Contract DE-AC36-08GO28308 with NREL.

The pathways to CVL study was supported by RePLACE (Redesigning Polymers to Leverage A Circular Economy), funded by the Office of Science of the U.S. Department of Energy via award # DE-SC0022290.

ICP-MS measurements MIT Center for Environmental Health Sciences, supported by a core center grant P30-ES002109 from the National Institute of Environmental Health Sciences, National Institutes of Health.

I would like to thank Dr. Jennifer Lewis for their synthesis of all of the hydrophobic BEA catalysts used in both studies presented here. I would like to additionally thank Dr. Helen Luo for their synthesis of the Sn-MCM-41 used in the CVL pathways project.

I would like to thank Reid Gilsdorf and Dr. Eswara Rao Chokkapu from Colorado State University for providing this project with the MVL to perform GC calibrations and Diels-Alder reaction studies.

Over the course of my time here at MIT, I have had a great set of mentors to help guide me on my projects.:

> To Soon Kwon: Thank you for helping to get me acclimated to the Román Lab when I first joined and for helping me set up my first experiments here. Thank you for becoming my mentor once again when I started to take over your safety officer duties.
>
> To Ydna Questell-Santiago: Thank you for introducing me to the world of reaction kinetics and cyclic lactones. My background in zeolite synthesis did not prepare me for the world of batch reactions and kinetic measurements, but your guidance helped me develop skills I used throughout my time here.
>
> To Alexi Khechfe: I really appreciate your willingness mentor me even as you neared the end of your PhD. Our discussions about research, both the actual work and all the additional stresses that come along with it, helped me as I hit roadblocks in my work and encouraged me to keep going.
>
> To Bowei Liu: Thank you for mentoring me through the end of my Master's thesis. Even as I was wrapping things up, you were still teaching me new techniques and methods. I appreciate the help you gave to push me to get this project to a point where I could write it up.

I want to give a shoutout to everyone who at one point shared the back corner of the office with me. I always looked forward to the discussions and jokes that would arise out of that group. It made coming into work so much better to have a great group to bounce ideas off of and take a break during long days of running reactions and working up data.

I want to thank the entire Plastics subgroup for cultivating a sense of comradery and allowing for great discussion over ideas in a space where I always felt free to share ideas and concerns about my projects. I always enjoyed getting to think through interesting results with everyone, even outside of scheduled subgroup meetings.

I want to extend a special thank you to Griffin Drake for being a great friend and mentor both in and out of the lab. Thank you for always taking time to talk to me when I was stuck with something and giving me

helpful advice on how to move past it. I could not have completed this thesis without your support, edits, and discussion. Thank you.

Finally, I would like to thank my thesis advisor, Professor Yuriy Román. I always looked forward to your passion for science and I left every meeting with you with a renewed sense of enthusiasm. Thank you for recruiting a great group of scientists who are always open to lending a hand and collaborate. I also wanted to show my appreciation for the care you show to your group by ensuring mental and physical health came before work.

Appendix: Supplementary Figures

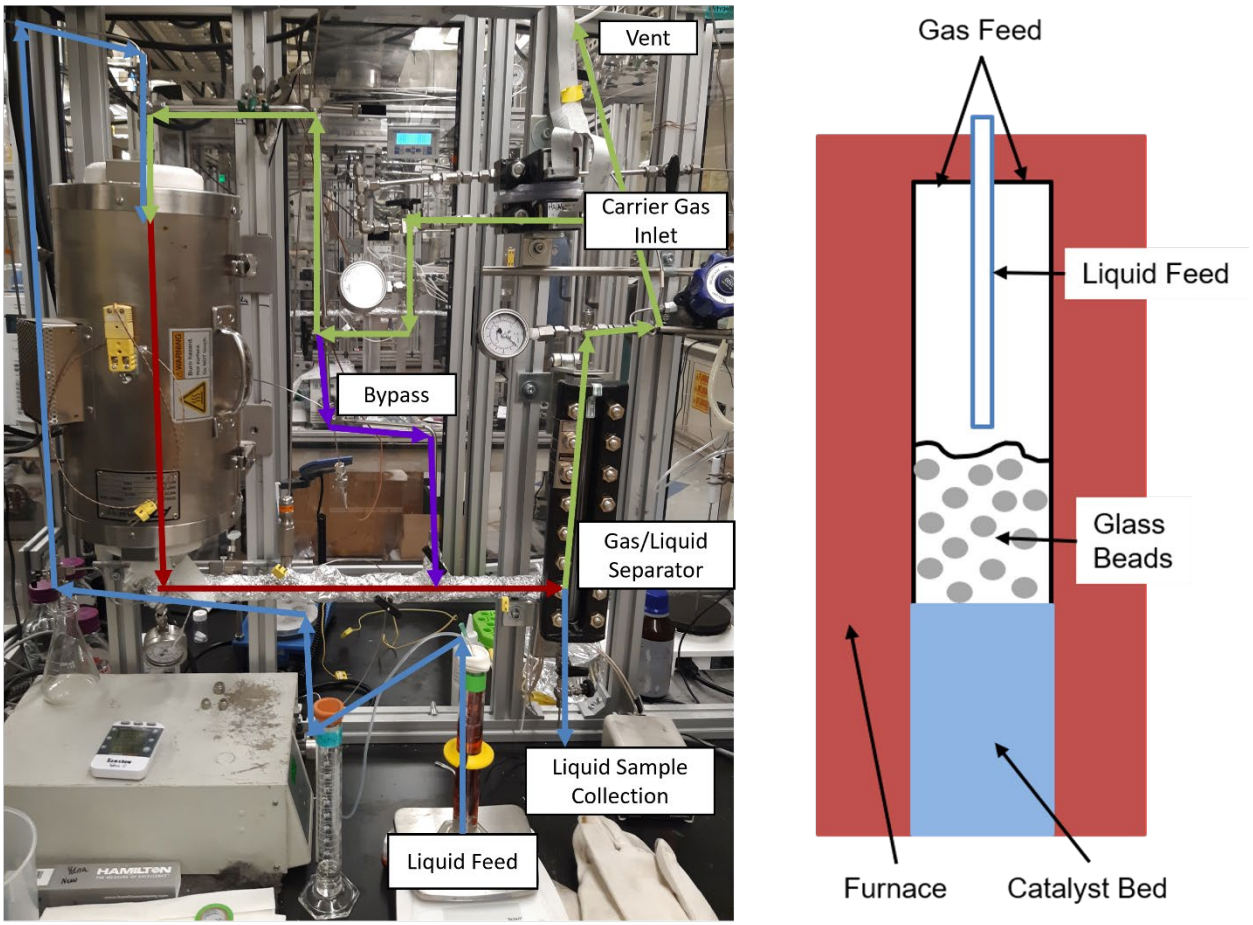

Figure A-1: Reactor image with line tracing for methyl lactate lactonization study

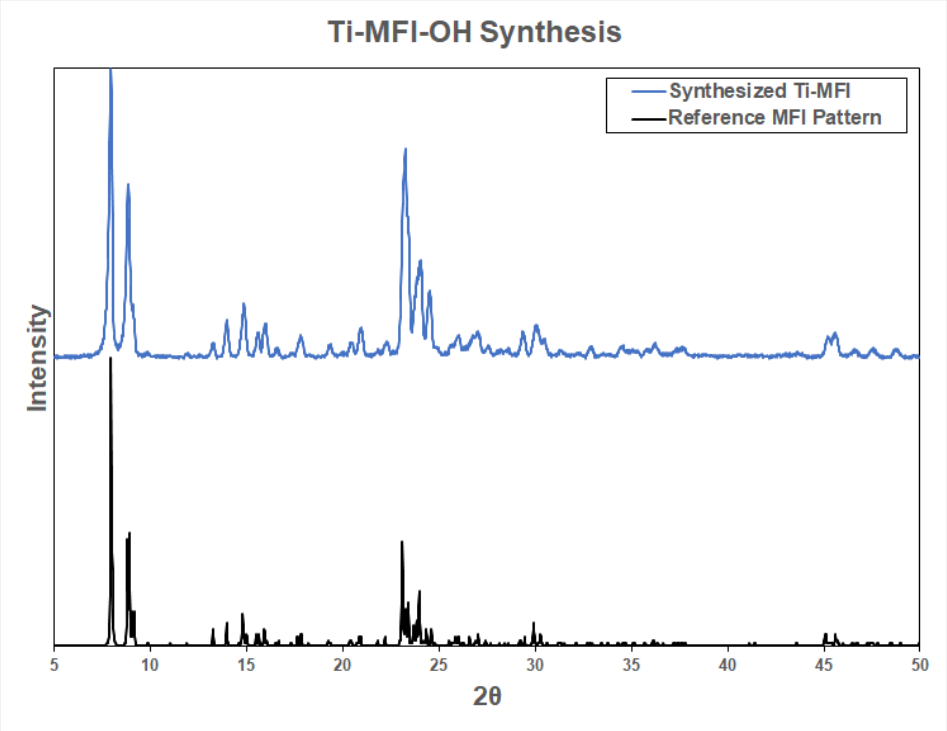

Figure A-2: XRD pattern of Ti-MFI synthesis compared to reference pattern (black)

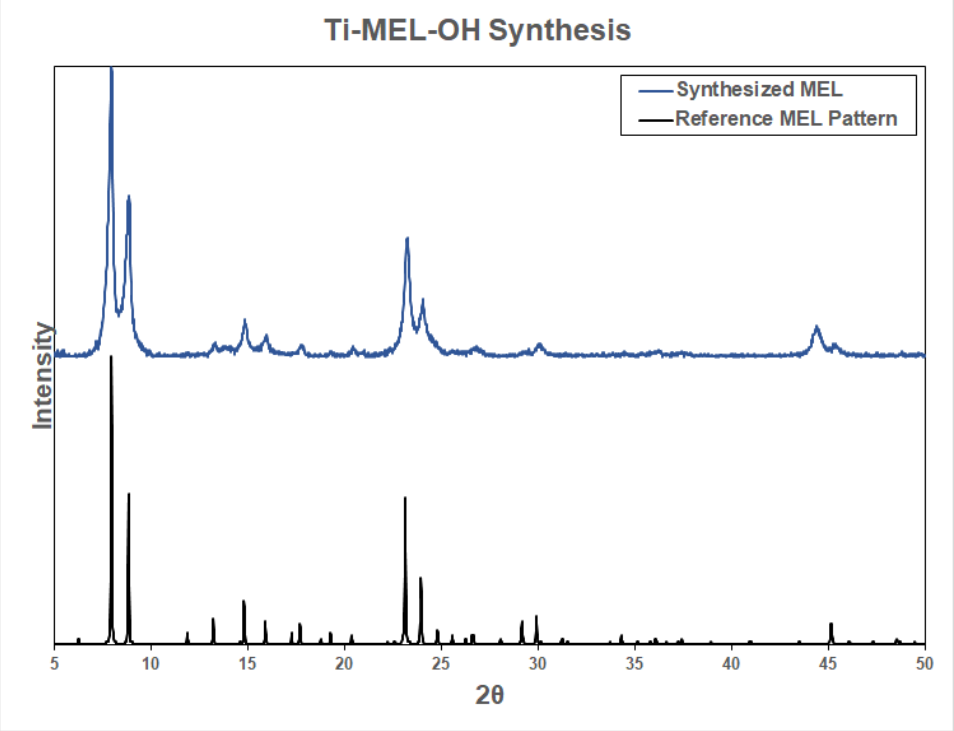

Figure A-3: XRD pattern of Ti-MEL synthesis compared to reference pattern (black)

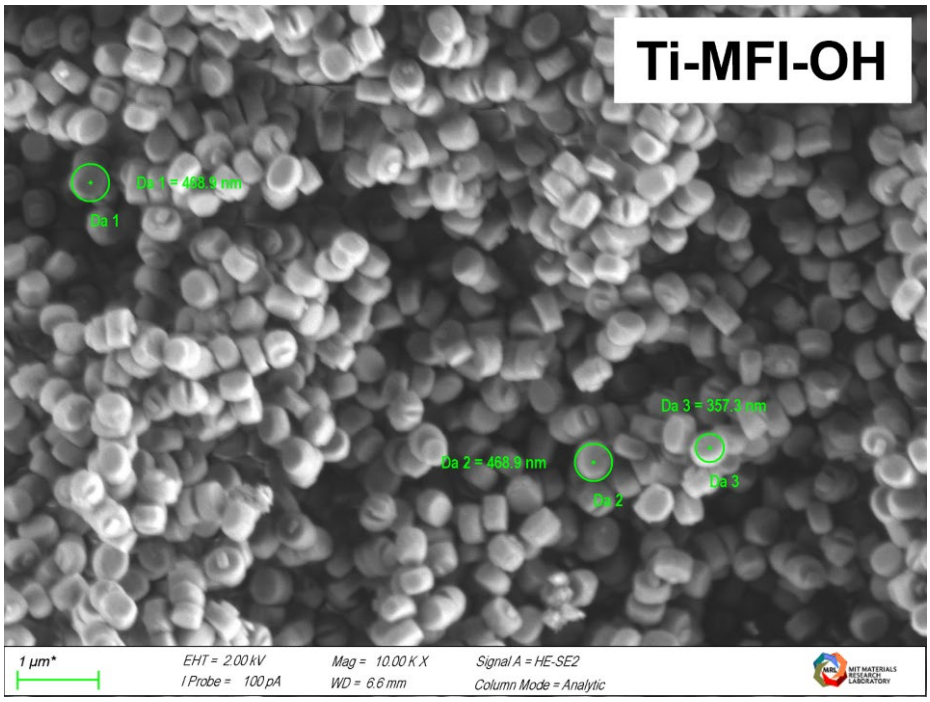

Figure A-4: SEM image of Ti-MFI-OH

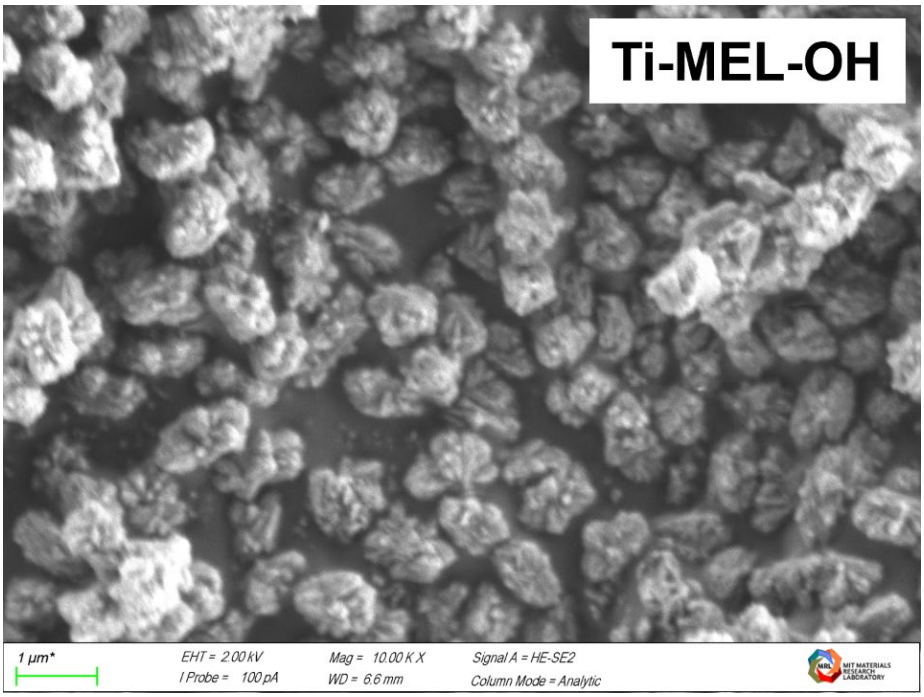

Figure A-5: SEM image of Ti-MEL-OH

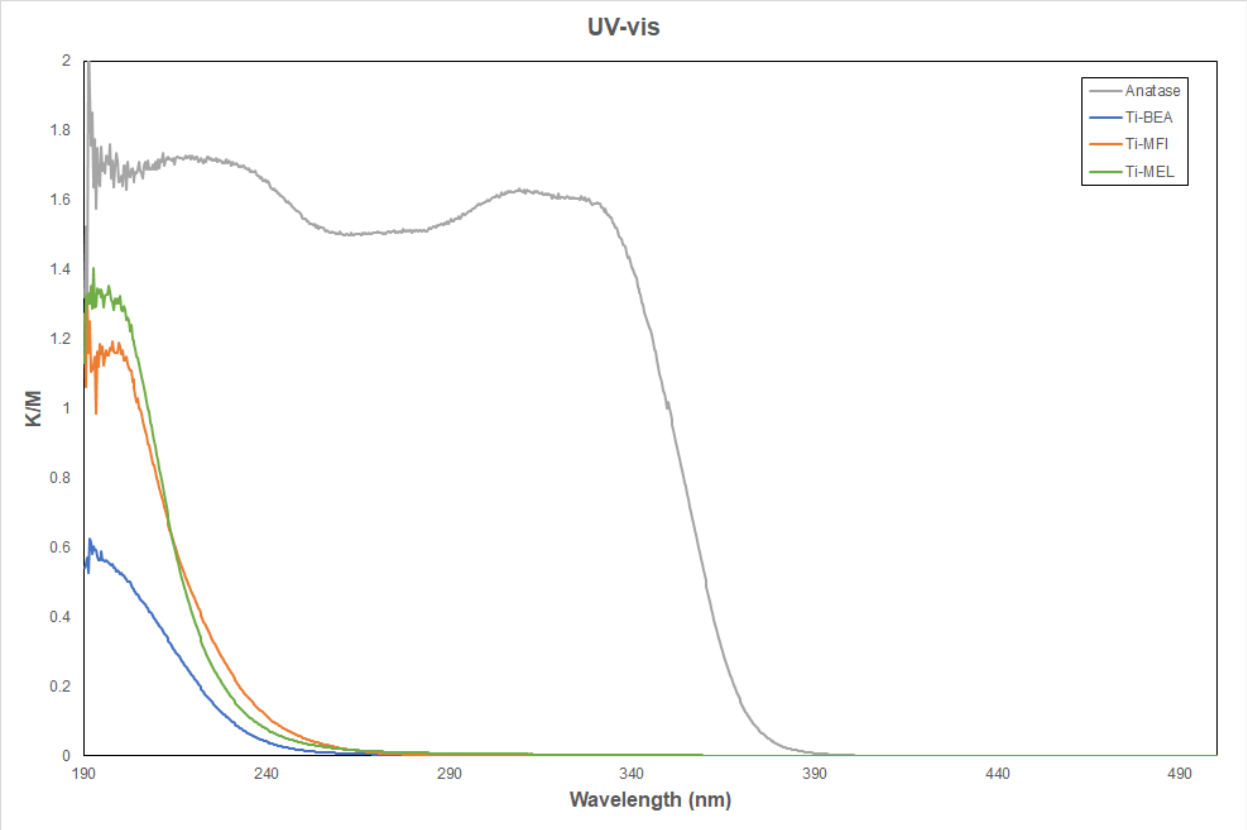

Figure A-6: UV-Vis spectra for Ti-BEA-F (blue), Ti-MFI-OH (orange), and Ti-MEL-OH (green). Compared to anatase (grey).

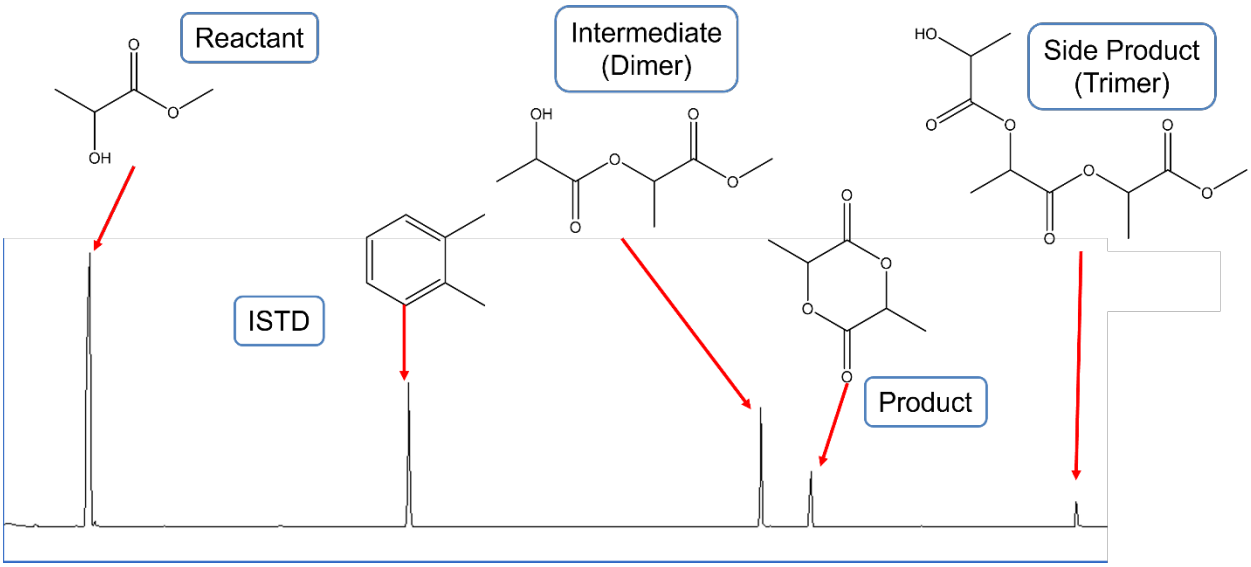

Figure A-7: Sample GC spectra highlighting the order in which species elute. This spectrum was taken from a reaction of neat methyl lactate flowing at 0.15 mL min^{-1} over 600 mg of Ti-BEA-F catalyst at 250 °C

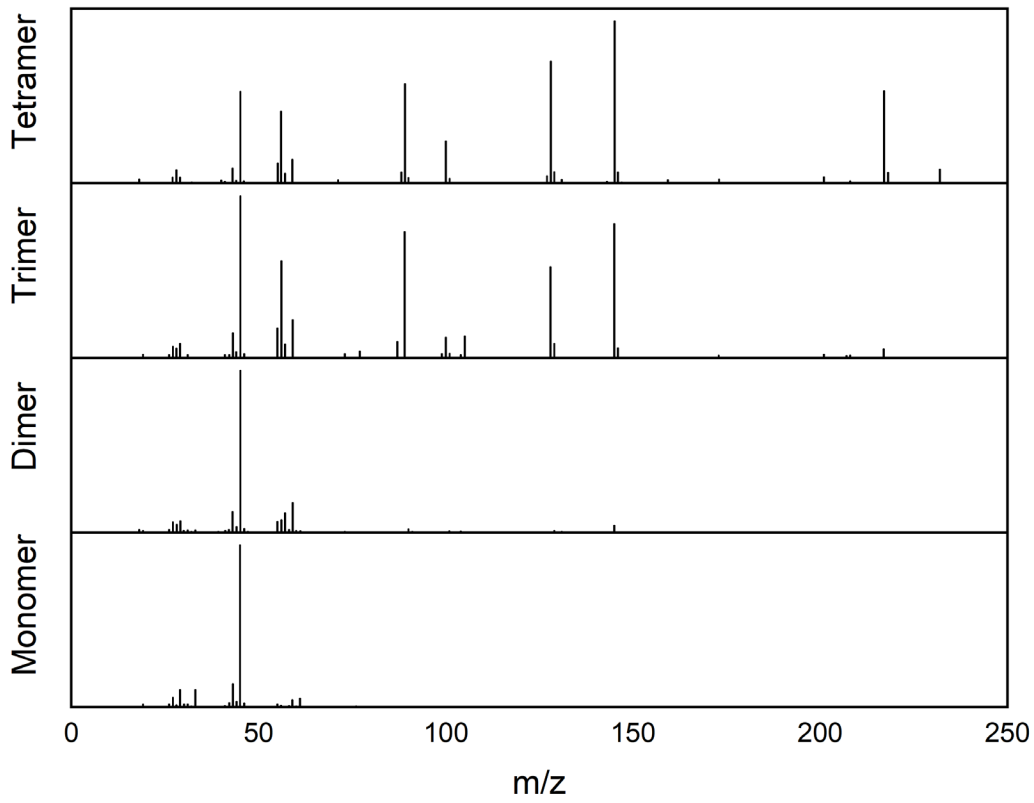

Figure A-8: GC-MS spectra for monomer (Methyl Lactate), dimer, trimer, and tetramer. Collected during a reactor cleanout performed by flowing acetone through an empty reactor.

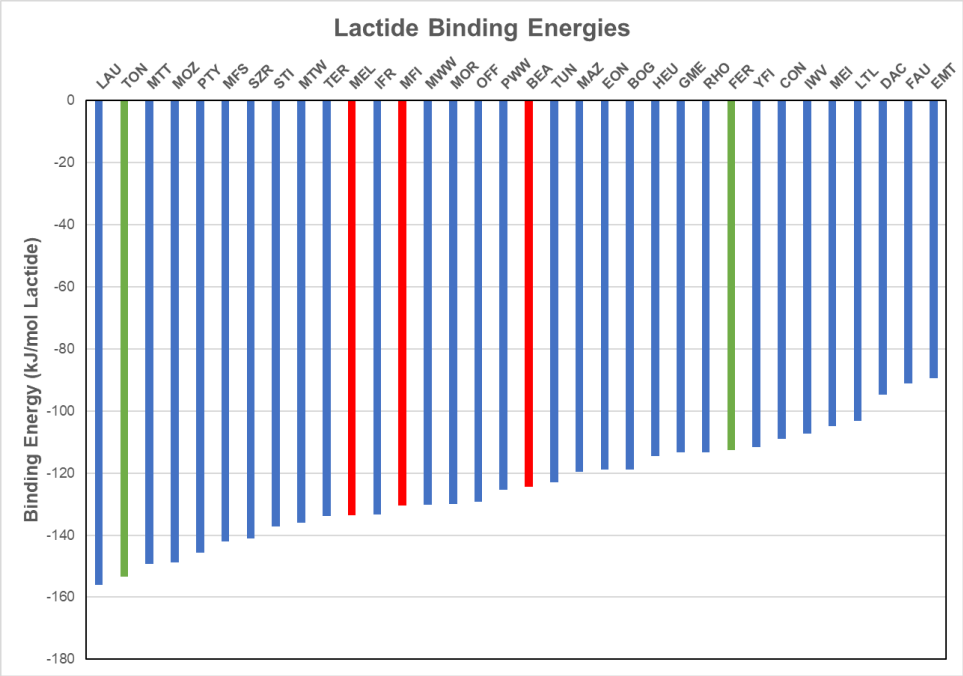

Figure A-9: Docking simulation results for lactide binding energies over all medium and larger pore zeolites experimentally synthesized in aluminosilicate form. Red were subjects of this study and green are prime candidate for future studies.

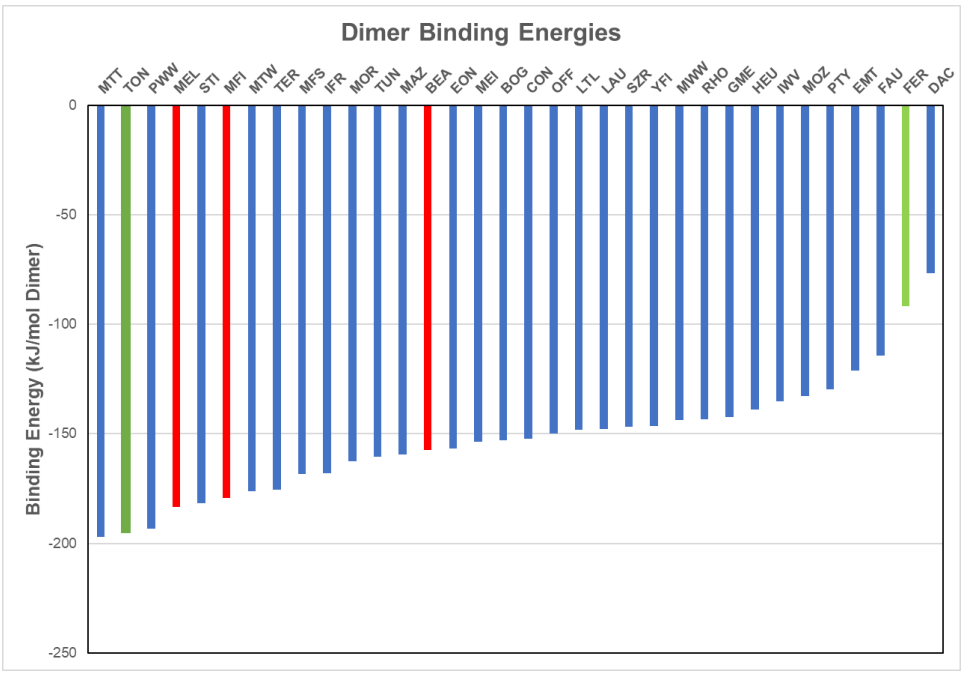

Figure A-10: Docking simulation results for dimer binding energies over all medium and larger pore zeolites experimentally synthesized in aluminosilicate form. Red were subjects of this study and green are prime candidate for future studies.

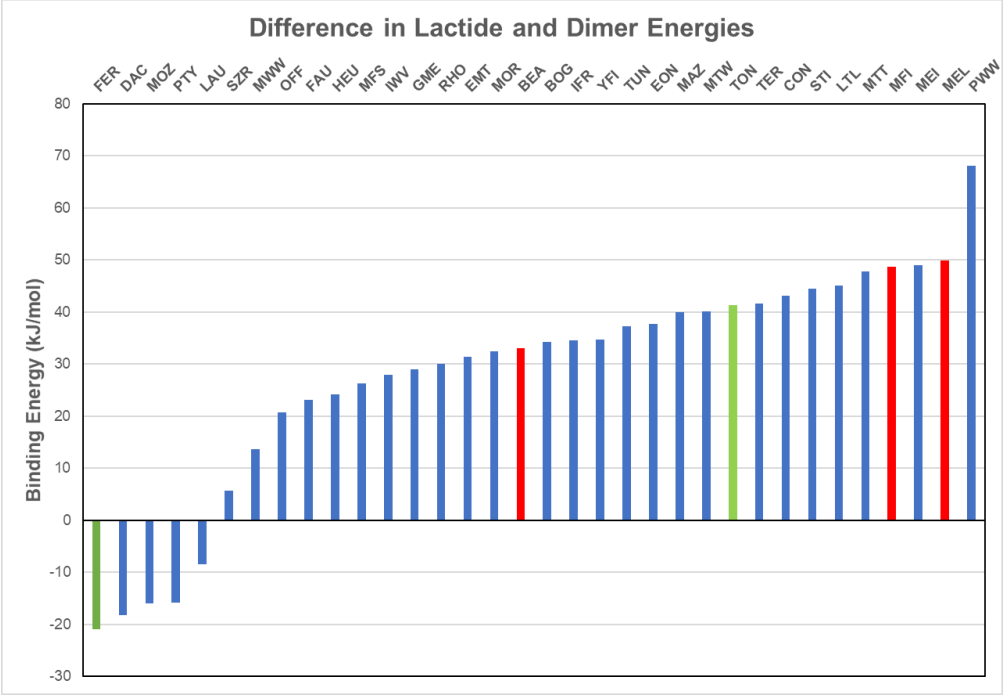

Figure A-11: Docking simulation results for difference in binding energies between the lactide and the dimer over all medium and larger pore zeolites experimentally synthesized in aluminosilicate form. Red were subjects of this study and green are prime candidate for future studies.

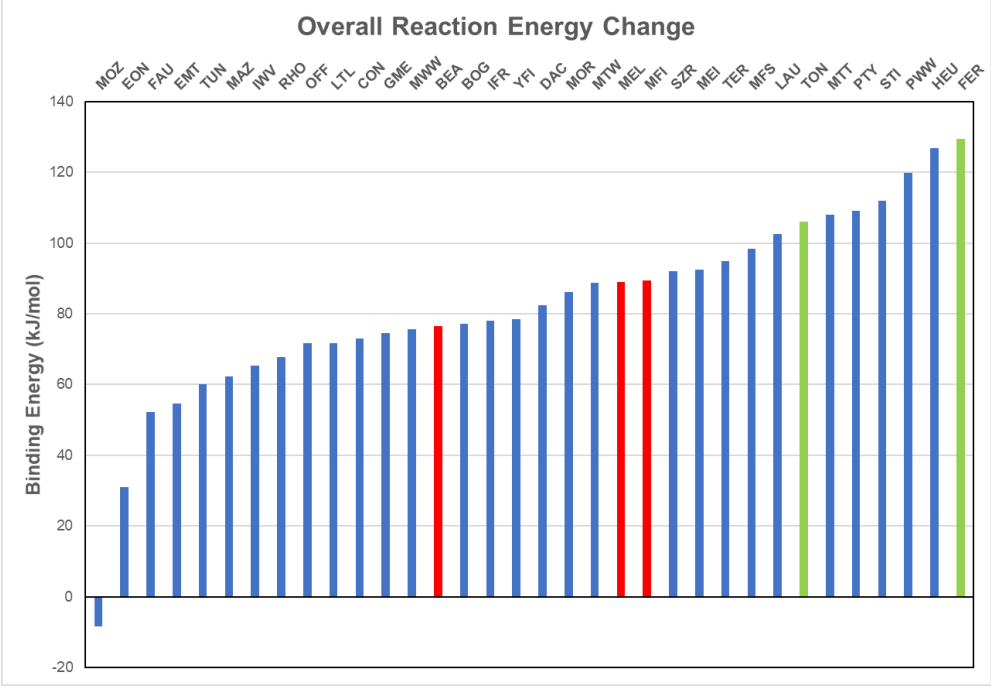

Figure A-12: Docking simulation results for overall binding energy change over all medium and larger pore zeolites experimentally synthesized in aluminosilicate form. Red were subjects of this study and green are prime candidate for future studies

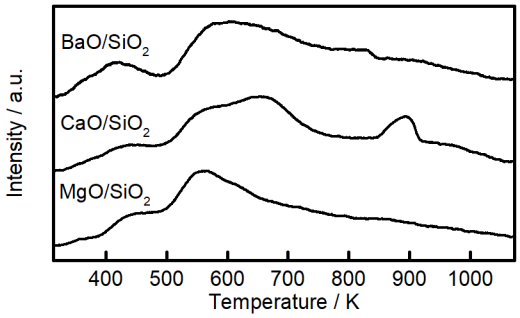

Figure A-13: CO_2 TPD of the three catalysts used in the aldol condensation of FA and DVL

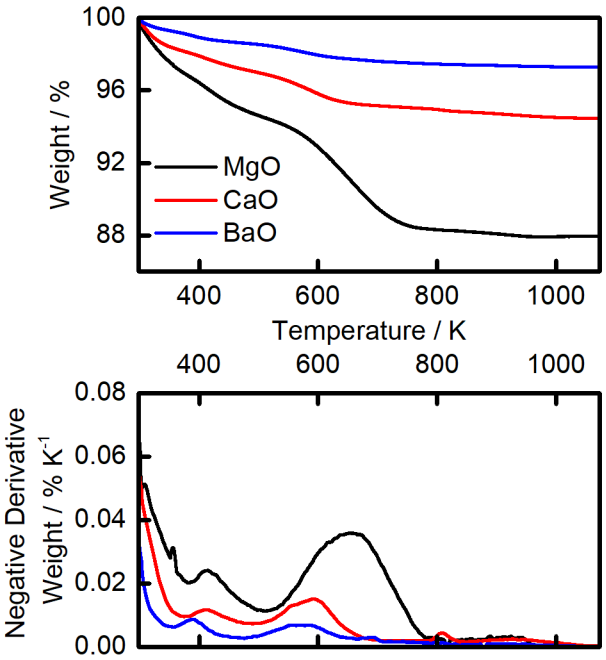

Figure A-14: TGA data for the 3 catalysts used in the aldol condensation of DVL and FA

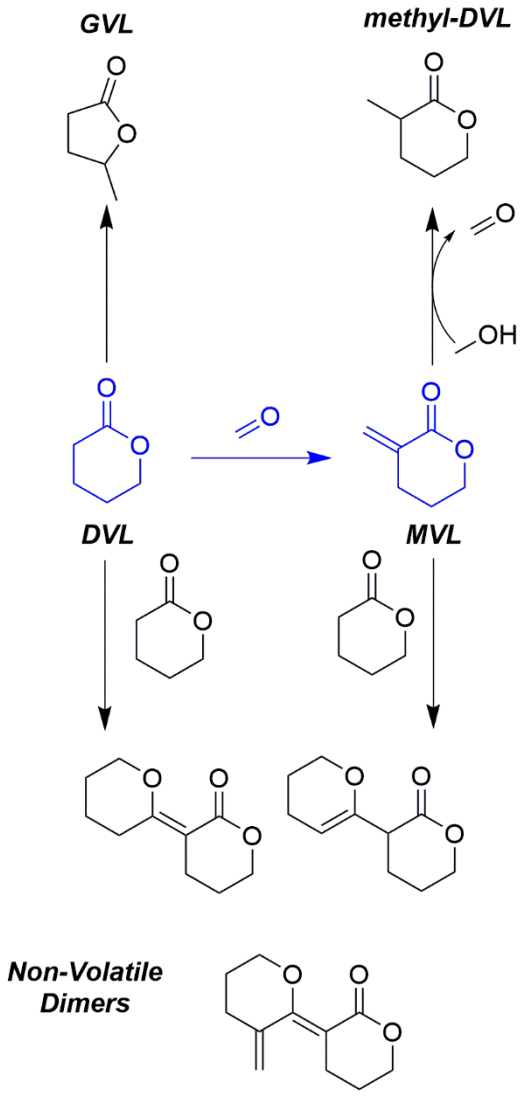

Figure A-15: Possible reaction pathways to non-volatile components in the aldol condensation of DVL and FA

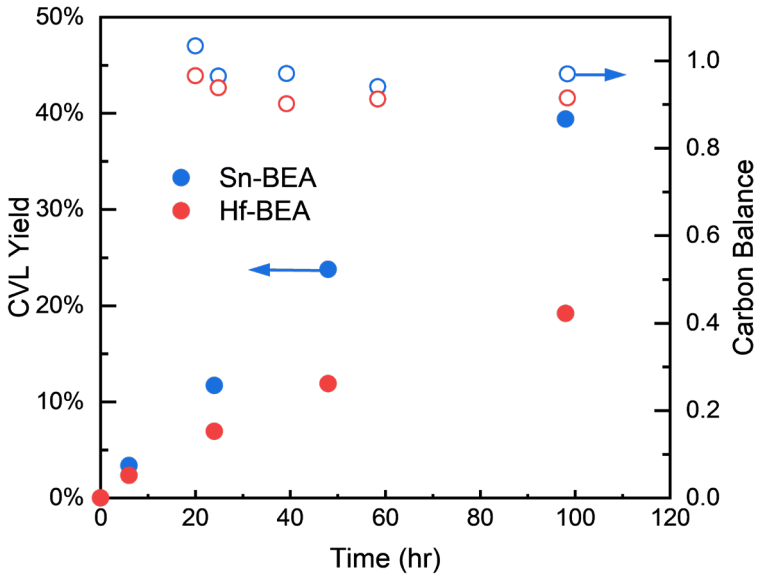

Figure A-16: Plot showing linear CVL yield with time up to 40% yield (approximately 40% MVL conversion). Reaction performed at room temperature with ~100 mg of M-BEA catalyst. 2 mmol MVL MVL:Butadiene ratio of 1:3. ~80% of the liquid by mass is toluene.

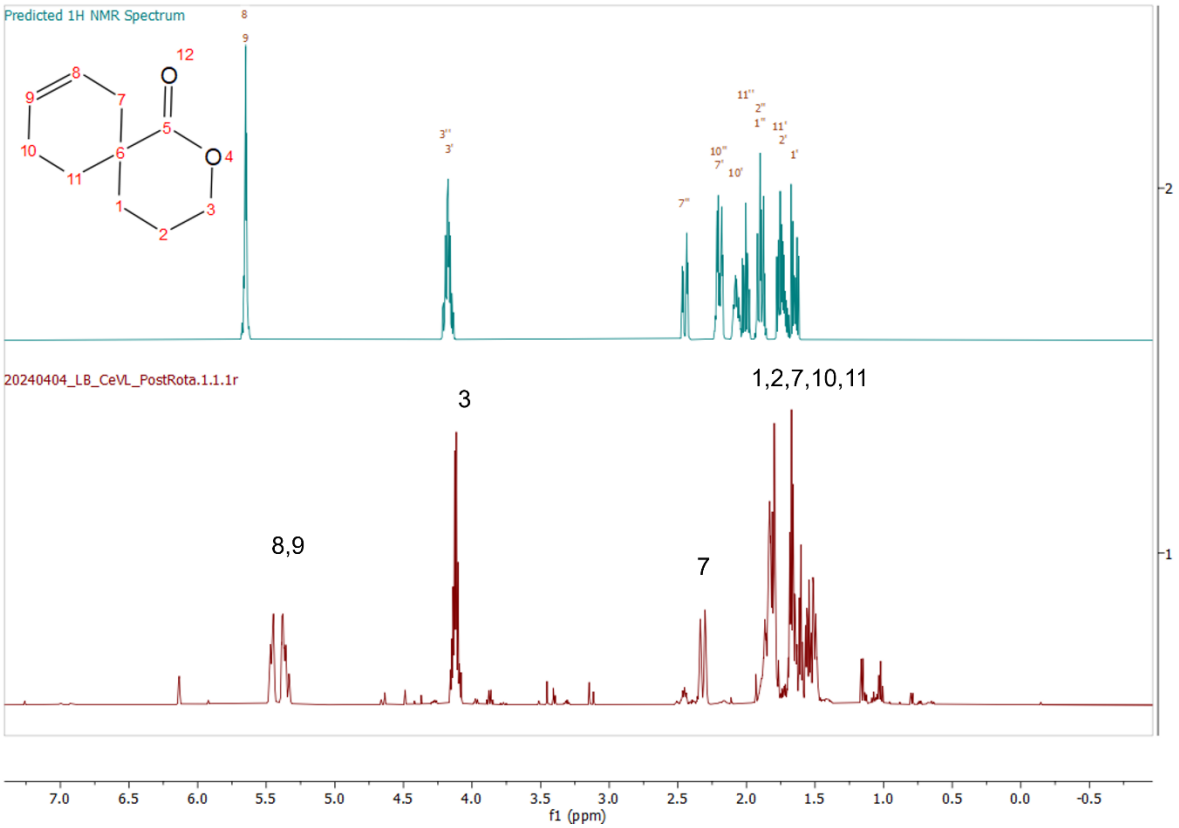

Figure A-17: [1]H-NMR of CeVL Product (bottom) compared to MestReNova predicted Spectrum (top)

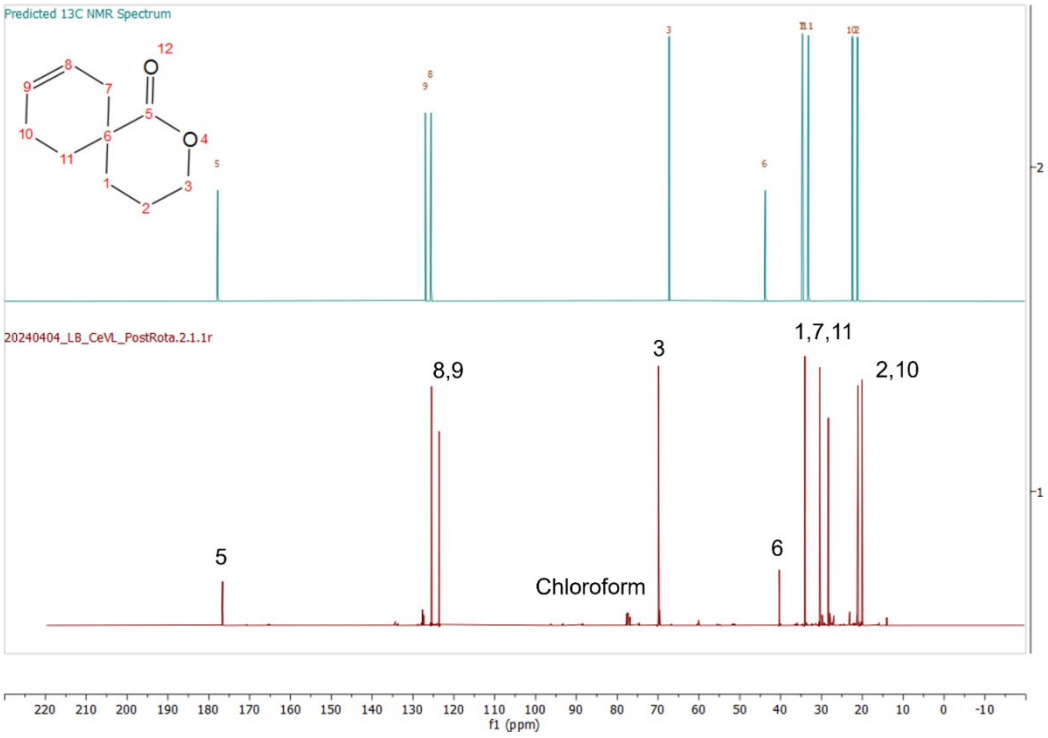

Figure A-18: ^{13}C-NMR of CeVL Product (bottom) compared to MestReNova predicted Spectrum (top)

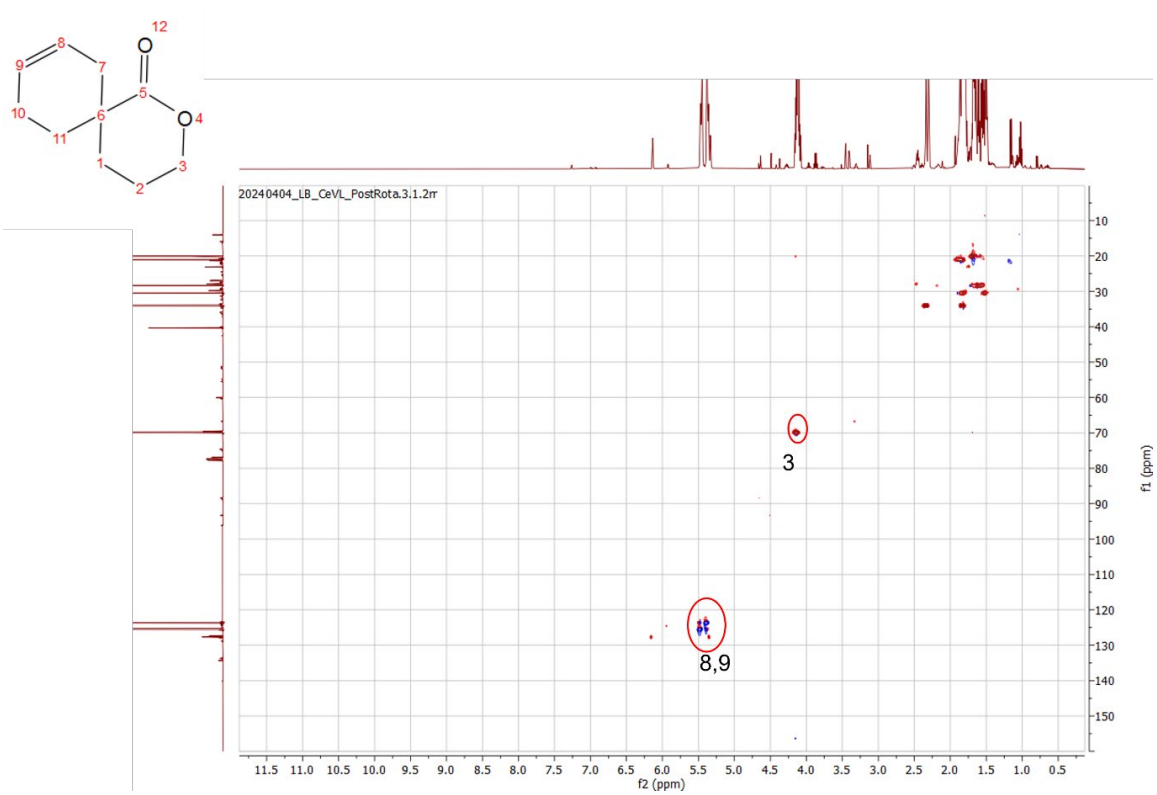

Figure A-19: HSQC of CeVL Product with important peaks circled and labeled.

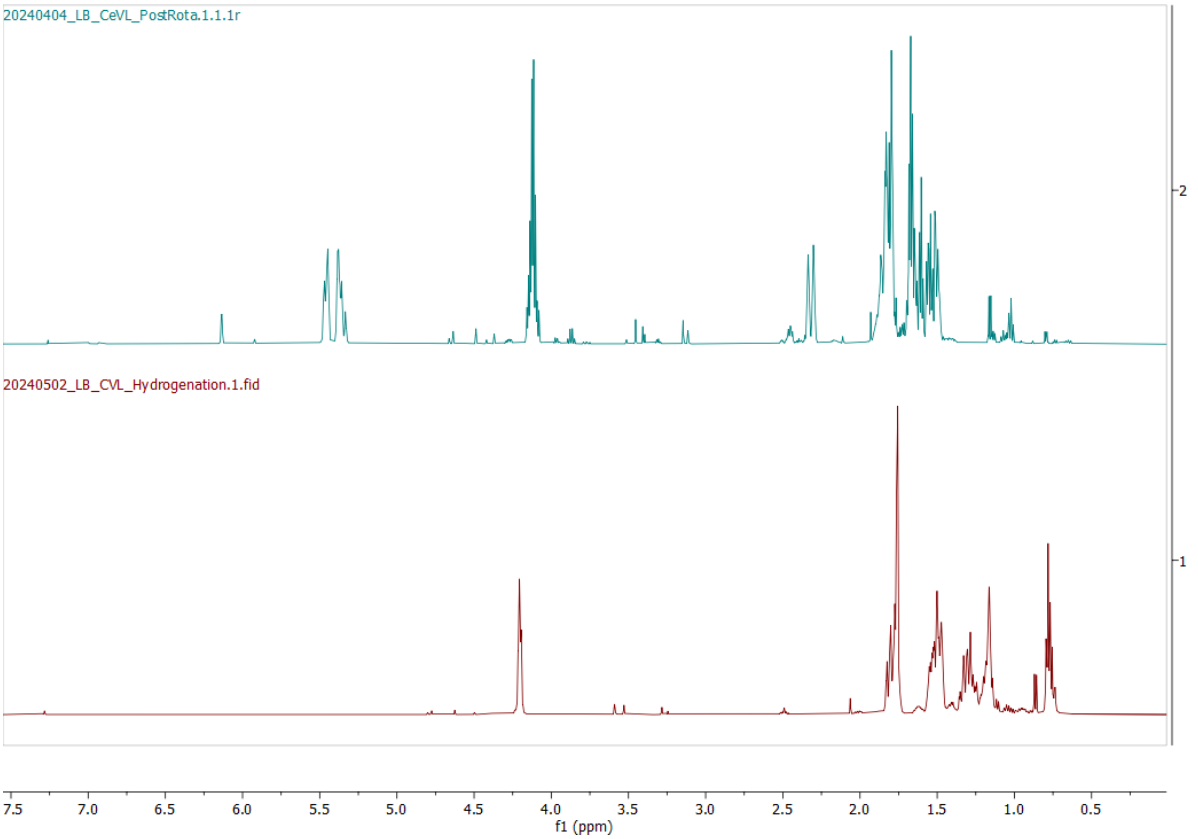

Figure A-20: ^{1}H-NMR comparison of CeVL (top) and CVL (bottom). After hydrogenation, peaks associated with C-C double bonds (5.5 ppm and 2.4 ppm) disappeared indicating successful hydrogenation.

References

1. Davis, M. E.; Lobo, R. F., Zeolite and molecular sieve synthesis. *Chem. Mater.* **1992,** *4* (4), 756-768.

2. Pérez Pariente, J.; Martínez Sánchez, M., Zeolites and ordered porous solids: fundamentals and applications. **2011**.

3. Cundy, C. S.; Cox, P. A., The hydrothermal synthesis of zeolites: history and development from the earliest days to the present time. *Chem. Rev.* **2003,** *103* (3), 663-702.

4. Kalló, D. n., Applications of Natural Zeolites in Water and Wastewater Treatment. *Rev. Mineral. Geochem.* **2001,** *45* (1), 519-550.

5. Kumar, S.; Srivastava, R.; Koh, J., Utilization of zeolites as CO2 capturing agents: Advances and future perspectives. *Journal of CO2 Utilization* **2020,** *41*, 101251.

6. *Zeolites Market by Type (Natural, Synthetic), Function (Ion-Exchange, Catalyst, Molecular Sieve), Synthetic Zeolites Application (Detergents, Absorbent, Catalysts), Natural Zeolites Application, and Region - Global Forecast to 2026* Markets and Markets, 2021.

7. Vermeiren, W.; Gilson, J.-P., Impact of zeolites on the petroleum and petrochemical industry. *Top. Catal.* **2009,** *52* (9), 1131-1161.

8. Davis, M. E., Ordered porous materials for emerging applications. *Nature* **2002,** *417* (6891), 813-821.

9. Gounder, R.; Moini, A., Automotive NO x abatement using zeolite-based technologies. *Reaction Chemistry & Engineering* **2019,** *4* (6), 966-968.

10. International Zeolite Association, Database of Zeolite Structures. http://europe.iza-structure.org/IZA-SC/ftc_table.php (accessed March 29, 2022).

11. Treacy, M.; Foster, M. http://www.hypotheticalzeolites.net/ (accessed March 29, 2022).

12. Tagiyev, D.; Azizov, A.; Starikov, R., Current Zeolites Application in the Oil Refining and Petroleum Industries. *Processes of Petrochemistry and Oil Refining* **2012,** *13* (3), 280-300.

13. Millini, R.; Perego, G.; Bellussi, G., Synthesis and characterization of boron-containing molecular sieves. *Top. Catal.* **1999,** *9* (1), 13-34.

14. Strohmaier, K. G.; Vaughan, D. E., Structure of the first silicate molecular sieve with 18-ring pore openings, ECR-34. *J. Am. Chem. Soc.* **2003,** *125* (51), 16035-16039.

15. Luo, H. Y.; Lewis, J. D.; Román-Leshkov, Y., Lewis acid zeolites for biomass conversion: Perspectives and challenges on reactivity, synthesis, and stability. *Annual review of chemical and biomolecular engineering* **2016,** *7*, 663-692.

16. Barrer, R. M., Synthesis of a zeolitic mineral with chabazite-like sorptive properties. *J. Chem. Soc.* **1948**, 127-132.

17. Barrer, R.; Hinds, L.; White, E., The hydrothermal chemistry of silicates. Part III. Reactions of analcite and leucite. *J. Chem. Soc.* **1953**, 1466-1475.

18. Matsukata, M.; Ogura, M.; Osaki, T.; Hari Prasad Rao, P. R.; Nomura, M.; Kikuchi, E., Conversion of dry gel to microporous crystals in gas phase. *Top. Catal.* **1999,** *9* (1), 77-92.

19. Cundy, C. S., Microwave techniques in the synthesis and modification of zeolite catalysts. A review. *Collection of Czechoslovak chemical communications* **1998,** *63* (11), 1699-1723.

20. Milton, R. M. Molecular Sieve Adsobents. April 14, 1959.

21. Barrer, R.; Denny, P., Hydrothermal chemistry of the silicates. Part IX. Nitrogenous aluminosilicates. *J. Chem. Soc.* **1961**, 971-982.

22. Burkett, S. L.; Davis, M. E., Mechanism of structure direction in the synthesis of Si-ZSM-5: an investigation by intermolecular 1H-29Si CP MAS NMR. *The Journal of Physical Chemistry* **1994,** *98* (17), 4647-4653.

23. Gies, H.; Marker, B., The structure-controlling role of organic templates for the synthesis of porosils in the systems SiO2/template/H2O. *Zeolites* **1992,** *12* (1), 42-49.

24. Di Iorio, J. R.; Nimlos, C. T.; Gounder, R., Introducing catalytic diversity into single-site chabazite zeolites of fixed composition via synthetic control of active site proximity. *ACS Catal.* **2017,** *7* (10), 6663-6674.

25. Gallego, E. M.; Li, C.; Paris, C.; Martín, N.; Martínez-Triguero, J.; Boronat, M.; Moliner, M.; Corma, A., Making Nanosized CHA Zeolites with Controlled Al Distribution for Optimizing Methanol-to-Olefin Performance. *Chemistry–A European Journal* **2018,** *24* (55), 14631-14635.

26. Hunger, M.; Kärger, J.; Pfeifer, H.; Caro, J.; Zibrowius, B.; Bülow, M.; Mostowicz, R., Investigation of internal silanol groups as structural defects in ZSM-5-type zeolites. *Journal of the Chemical Society, Faraday Transactions 1: Physical Chemistry in Condensed Phases* **1987,** *83* (11), 3459-3468.

27. Villaescusa, L. A.; Barrett, P. A.; Camblor, M. A., ITQ-7: A New Pure Silica Polymorph with a Three-Dimensional System of Large Pore Channels. *Angew. Chem. Int. Ed.* **1999,** *38* (13-14), 1997-2000.

28. Di Iorio, J. R.; Johnson, B. A.; Román-Leshkov, Y., Ordered hydrogen-bonded alcohol networks confined in Lewis acid zeolites accelerate transfer hydrogenation turnover rates. *J. Am. Chem. Soc.* **2020,** *142* (45), 19379-19392.

29. Bates, J. S.; Gounder, R., Kinetic effects of molecular clustering and solvation by extended networks in zeolite acid catalysis. *Chemical Science* **2021,** *12* (13), 4699-4708.

30. Bregante, D. T.; Chan, M. C.; Tan, J. Z.; Ayla, E. Z.; Nicholas, C. P.; Shukla, D.; Flaherty, D. W., The shape of water in zeolites and its impact on epoxidation catalysis. *Nature Catalysis* **2021,** *4* (9), 797-808.

31. Derouane, E. G., Zeolites as solid solvents. *J. Mol. Catal. A: Chem.* **1998,** *134* (1-3), 29-45.

32. Gounder, R.; Iglesia, E., The catalytic diversity of zeolites: confinement and solvation effects within voids of molecular dimensions. *Chem. Commun.* **2013,** *49* (34), 3491-3509.

33. Snyder, B. E.; Bols, M. L.; Schoonheydt, R. A.; Sels, B. F.; Solomon, E. I., Iron and copper active sites in zeolites and their correlation to metalloenzymes. *Chem. Rev.* **2017,** *118* (5), 2718-2768.

34. Van de Vyver, S.; Román-Leshkov, Y., Metalloenzyme-Like Zeolites as Lewis Acid Catalysts for C□ C Bond Formation. *Angew. Chem. Int. Ed.* **2015,** *54* (43), 12554-12561.

35. Harris, J. W.; Liao, W.-C.; Di Iorio, J. R.; Henry, A. M.; Ong, T.-C.; Comas-Vives, A.; Coperet, C.; Gounder, R., Molecular structure and confining environment of Sn sites in single-site chabazite zeolites. *Chem. Mater.* **2017,** *29* (20), 8824-8837.

36. Grosso-Giordano, N. A.; Hoffman, A. S.; Boubnov, A.; Small, D. W.; Bare, S. R.; Zones, S. I.; Katz, A., Dynamic reorganization and confinement of TiIV active sites controls olefin epoxidation catalysis on two-dimensional zeotypes. *J. Am. Chem. Soc.* **2019,** *141* (17), 7090-7106.

37. Gounder, R.; Iglesia, E., The roles of entropy and enthalpy in stabilizing ion-pairs at transition states in zeolite acid catalysis. *Acc. Chem. Res.* **2012,** *45* (2), 229-238.

38. Bregante, D. T.; Tan, J. Z.; Sutrisno, A.; Flaherty, D. W., Heteroatom substituted zeolite FAU with ultralow Al contents for liquid-phase oxidation catalysis. *Catal. Sci. Technol.* **2020,** *10* (3), 635-647.

39. Cordon, M. J.; Vega-Vila, J. C.; Casper, A.; Huang, Z.; Gounder, R., Tighter Confinement Increases Selectivity of d-Glucose Isomerization Toward l-Sorbose in Titanium Zeolites. *Angew. Chem. Int. Ed.* **2020,** *59* (43), 19102-19107.

40. Li, C.; Paris, C.; Martínez-Triguero, J.; Boronat, M.; Moliner, M.; Corma, A., Synthesis of reaction-adapted zeolites as methanol-to-olefins catalysts with mimics of reaction intermediates as organic structure-directing agents. *Nature Catalysis* **2018,** *1* (7), 547-554.

41. Gallego, E. M.; Portilla, M. T.; Paris, C.; León-Escamilla, A.; Boronat, M.; Moliner, M.; Corma, A., "Ab initio" synthesis of zeolites for preestablished catalytic reactions. *Science* **2017,** *355* (6329), 1051-1054.

42. Schwalbe-Koda, D.; Gómez-Bombarelli, R., Benchmarking binding energy calculations for organic structure-directing agents in pure-silica zeolites. *J. Chem. Phys.* **2021,** *154* (17), 174109.

43. Schwalbe-Koda, D.; Kwon, S.; Paris, C.; Bello-Jurado, E.; Jensen, Z.; Olivetti, E.; Willhammar, T.; Corma, A.; Román-Leshkov, Y.; Moliner, M., A priori control of zeolite phase competition and intergrowth with high-throughput simulations. *Science* **2021,** *374* (6565), 308-315.

44. *The New Plastics Economy - Rethinking the Future of Plastics*; Ellen MacArthur Foundation and McKinsey & Company: World Economic Forum, 2016.

45. Hong, M.; Chen, E. Y.-X., Future directions for sustainable polymers. *Trends in Chemistry* **2019,** *1* (2), 148-151.

46. Schneiderman, D. K.; Hillmyer, M. A., 50th anniversary perspective: There is a great future in sustainable polymers. *Macromolecules* **2017,** *50* (10), 3733-3749.

47. Geyer, R.; Jambeck, J. R.; Law, K. L., Production, use, and fate of all plastics ever made. *Science Advances* **2017,** *3* (7), e1700782.

48. Hong, M.; Chen, E. Y.-X., Chemically recyclable polymers: a circular economy approach to sustainability. *Green Chem.* **2017,** *19* (16), 3692-3706.

49. Dainton, F.; Ivin, K., Reversibility of the propagation reaction in polymerization processes and its manifestation in the phenomenon of a 'Ceiling Temperature'. *Nature* **1948,** *162* (4122), 705-707.

50. Shi, C.; Reilly, L. T.; Kumar, V. S. P.; Coile, M. W.; Nicholson, S. R.; Broadbelt, L. J.; Beckham, G. T.; Chen, E. Y.-X., Design principles for intrinsically circular polymers with tunable properties. *Chem* **2021,** *7* (11), 2896-2912.

51. Castro-Aguirre, E.; Iñiguez-Franco, F.; Samsudin, H.; Fang, X.; Auras, R., Poly(lactic acid)—Mass production, processing, industrial applications, and end of life. *Adv. Drug Delivery Rev.* **2016,** *107*, 333-366.

52. Van Wouwe, P.; Dusselier, M.; Vanleeuw, E.; Sels, B., Lactide synthesis and chirality control for polylactic acid production. *ChemSusChem* **2016,** *9* (9), 907-921.

53. Dechy-Cabaret, O.; Martin-Vaca, B.; Bourissou, D., Controlled ring-opening polymerization of lactide and glycolide. *Chem. Rev.* **2004,** *104* (12), 6147-6176.

54. Kopinke, F.-D.; Remmler, M.; Mackenzie, K.; Möder, M.; Wachsen, O., Thermal decomposition of biodegradable polyesters—II. Poly (lactic acid). *Polym. Degrad. Stab.* **1996,** *53* (3), 329-342.

55. Hong, M.; Chen, E. Y.-X., Completely recyclable biopolymers with linear and cyclic topologies via ring-opening polymerization of γ-butyrolactone. *Nature Chem.* **2016,** *8* (1), 42-49.

56. Tang, X.; Chen, E. Y.-X., Chemical synthesis of perfectly isotactic and high melting bacterial poly (3-hydroxybutyrate) from bio-sourced racemic cyclic diolide. *Nat. Commun.* **2018,** *9* (1), 1-11.

57. De Clercq, R.; Dusselier, M.; Poleunis, C.; Debecker, D. P.; Giebeler, L.; Oswald, S.; Makshina, E.; Sels, B. F., Titania-silica catalysts for lactide production from renewable alkyl lactates: structure–activity relations. *ACS Catal.* **2018,** *8* (9), 8130-8139.

58. Camblor, M. A.; Villaescusa, L. A.; Díaz-Cabañas, M. J., Synthesis of all-silica and high-silica molecular sieves in fluoride media. *Topics in Catalysis* **1999,** *9* (1), 59-76.

59. Sudhakar Reddy, J.; Kumar, R., Crystallization kinetics of a new titanium silicate with MEL structure (TS-2). *Zeolites* **1992,** *12* (1), 95-100.

60. Scanlon, J. T.; Willis, D. E., Calculation of Flame Ionization Detector Relative Response Factors Using the Effective Carbon Number Concept. *J. Chromatogr. Sci.* **1985,** *23* (8), 333-340.

61. Kustova, M. Y.; Hasselriis, P.; Christensen, C. H., Mesoporous MEL – Type Zeolite Single Crystal Catalysts. *Catalysis Letters* **2004,** *96* (3), 205-211.

62. Tuel, A.; Ben Taârit, Y., Synthesis, characterization, and catalytic properties of titanium silicates prepared using phosphonium ions. *Zeolites* **1993,** *13* (5), 357-364.

63. Johnson, B. A.; Di Iorio, J. R.; Román-Leshkov, Y., Identification and quantification of distinct active sites in Hf-Beta zeolites for transfer hydrogenation catalysis. *J. Catal.* **2021,** *404*, 607-619.

64. De Clercq, R.; Dusselier, M.; Makshina, E.; Sels, B. F., Catalytic Gas-Phase Production of Lactide from Renewable Alkyl Lactates. *Angew. Chem. Int. Ed.* **2018,** *57* (12), 3074-3078.

65. Manzer, L. E., Catalytic synthesis of α-methylene-γ-valerolactone: a biomass-derived acrylic monomer. *Appl. Catal., A* **2004,** *272* (1), 249-256.

66. Settle, A. E.; Berstis, L.; Rorrer, N. A.; Roman-Leshkóv, Y.; Beckham, G. T.; Richards, R. M.; Vardon, D. R., Heterogeneous Diels–Alder catalysis for biomass-derived aromatic compounds. *Green Chem.* **2017,** *19* (15), 3468-3492.

67. Khechfe, A. A.; Matha, T. B. M.; Román-Leshkov, Y., Solvent Polarity and Framework Hydrophobicity of Hf-BEA Zeolites Influence Aldol Addition Rates in Organic Media. *ACS Catal.* **2023,** *13* (9), 6474-6485.

68. Luo, H. Y.; Bui, L.; Gunther, W. R.; Min, E.; Román-Leshkov, Y., Synthesis and Catalytic Activity of Sn-MFI Nanosheets for the Baeyer–Villiger Oxidation of Cyclic Ketones. *ACS Catal.* **2012,** *2* (12), 2695-2699.

69. Chen, M.; Liang, C.; Zhang, F.; Li, H., Periodic Mesoporous Silica-Supported Scandium Triflate as a Robust and Reusable Lewis Acid Catalyst for Carbon–Carbon Coupling Reactions in Water. *ACS Sustainable Chemistry & Engineering* **2014,** *2* (3), 486-492.

70. Wang, Y.; Lewis, J. D.; Román-Leshkov, Y., Synthesis of Itaconic Acid Ester Analogues via Self-Aldol Condensation of Ethyl Pyruvate Catalyzed by Hafnium BEA Zeolites. *ACS Catal.* **2016,** *6* (5), 2739-2744.

71. Lenz, T. G.; Vaughan, J. D., Force field calculation of equilibrium thermodynamic properties: Diels–Alder reaction of 1,3-butadiene and ethylene and Diels–Alder dimerization of 1,3-butadiene. *J. Comput. Chem.* **1990,** *11* (3), 351-360.

72. Hammond, C.; Conrad, S.; Hermans, I., Simple and Scalable Preparation of Highly Active Lewis Acidic Sn-β. *Angew. Chem. Int. Ed.* **2012,** *51* (47), 11736-11739.

73. Schmidt, B.; Wolf, F.; Ehlert, C., Systematic Investigation into the Matsuda–Heck Reaction of α-Methylene Lactones: How Conformational Constraints Direct the β-H-Elimination Step. *J. Org. Chem.* **2016,** *81* (22), 11235-11249.

74. Onaka, M.; Hashimoto, N.; Kitabata, Y.; Yamasaki, R., Aluminum-rich mesoporous aluminosilicate (Al-HMS) as a solid acid catalyst for the Diels–Alder reaction of acrylates with 1,3-dienes. *Appl. Catal., A* **2003,** *241* (1), 307-317.